2017

COMPARISON OF AMBIENT NOISE METHODS TO FIND SURFACE - WAVE DISPERSION CURVES AT PACAYA VOLCANO, GUATEMALA

Simone Puel
Michigan Technological University, spuel@mtu.edu

COMPARISON OF AMBIENT NOISE METHODS TO FIND SURFACE - WAVE DISPERSION CURVES AT PACAYA VOLCANO, GUATEMALA

By

Simone Puel

A THESIS

Submitted in partial fulfillment of the requirements for the degree of

MASTER OF SCIENCE

In Geology

MICHIGAN TECHNOLOGICAL UNIVERSITY

2017

This thesis has been approved in partial fulfillment of the requirements for the Degree of MASTER OF SCIENCE in Geology.

Department of Geological and Mining Engineering and Sciences

Thesis Advisor:	*Dr. Gregory P. Waite*
Committee Member:	*Dr. Alessandro Tibaldi*
Committee Member:	*Dr. Simon A. Carn*
Department Chair:	*Dr. John S. Gierke*

Contents

List of Figures

List of Tables

Acknowledgments

There are many people to whom I would like to thank, not only for the achievement of this work, but also for this incredible year spent in Houghton, at Michigan Tech. Firstly, I am really sure that the possibility of studying a year of your life abroad in a different academic environment is the best opportunity that any university can offer. For this reason, I would like to thank the coordinators and all people who have thought and made this *INVOGE (International Geological Masters in Volcanology and Geotechniques)* program possible.

I wish to thank Michigan Technological University for the huge opportunity offered to me this year. I found kindly people everywhere, professionalism and immediate solutions for any encountered problem.

I express my immense gratitude to Greg Waite, my advisor and my academic guide, to whom I have a deep respect and admiration. His encouragement and patience towards me were determinant to make this effort possible. Moreover, he conveyed me his great passion for volcano seismology, teaching me the principles of seismology and understanding volcano behaviors.

Thanks to Federica Lanza for the useful advice about seismicity at Pacaya volcano and her first paper on SPAC through a seismic array employed at Pacaya in 2011. She was always available to help me to solve any issue about MATLAB codes.

Thanks to all people of the Volcano Geophysics group (Greg, Fede, Kyle, Hans, Max and Monica) for the seismic data collected in 2015 field campaign and for discussing all studies and improvements about Guatemalan volcanoes. Moreover, it represented the first research group whose I was involved and for this reason thank you very much.

Thanks to GMES including all students who I met, all professors and all people (John, Kelly, Brittany, ...) who work with passion and dedication to help students to realize their dreams. I felt immediately like in a family.

Thanks to University of Milano-Bicocca for having taught and introduced me to Geology and Volcanology. Moreover thanks for this great opportunity of double degree, in particular professor Alessandro Tibaldi for the useful advice.

A really thanks to my parents (Bruno and Fiorella), my brother Matteo and my grandma Maria, because without them I would not be here.

Thanks also to all my friends, Italian (Andrea, Diletta, all "Candela" group, Salvatore, Riccardo, Luigi, Lorenzo, ...) and all friends who I met in Houghton (Tri, Lopa, Leo, Lauren, Joe, Christie, Lukasz, Arya, ...) because they helped me a lot in all kind of situations and the happy moments spent together.

Abstract

The application of ambient noise analysis to active volcanic systems represents a recent technique to model seismic structure without distinct sources. All the existing methods are based on the fact that surface waves are dispersive and most of them require a large number of available days and inter-station distances larger than 2-3 wavelengths. We apply multiple techniques to seismic data recorded during a temporary deployment of 19 seismic stations in January 2015 at Pacaya volcano, Guatemala, a dataset with some distinct differences from those typically used for ambient noise analysis. Despite having less than a week of data and relatively close inter-station spacing, we find a good agreement between the approaches. In particular, we find that the SPAC method (Aki, 1957) is applicable not only for a seismic array, but also for single pairs of stations. It may be particularly favorable in those conditions characterized by small set of data and small inter-station distances. We also noted linear relationship between phase velocity and inter-station distance might suggest a contribution of body/scattered waves within the surface waves and it is probably due to the seismic station configuration in proximity of the Pacaya vent.

Introduction

The original purpose of this study was to create a 3D seismic velocity tomographic model of Pacaya volcano, Guatemala using ambient seismic noise. Pacaya is an active volcano and has had at least one major flank collapse in the past, so characterizing the structure is important for hazard mitigation.

In active volcanic areas, we can expect that large variations in the wave speed are very common. In fact, the presence of unconsolidated tephra, loose sediments, emplacement of dikes and melted rocks produce rapid changes in seismic velocity. A major limitation of most types of seismic tomography studies is that distinct seismic sources are required. For example, in P-wave tomography the inversion of travel times from earthquakes or other known sources can be used to determine the 3D structure in volume containing the events and stations. While these sources can be either natural or artificial, the quality of the model depends on the distribution of these sources.

In ambient noise tomography, instead, seismic structure can be obtained from the random, diffuse wave-field. No individual, distinct sources are required. Instead a representation of the wave that passes between a pair of stations can be determined using cross-correlation of ambient noise. Because surface waves generally have larger amplitudes than body waves, this approach is particularly suited to surface waves analysis. Surface waves are dispersive. That is, waves with different frequencies travel with different velocities. These two parameters, velocity and frequency, are related by the so-called *phase* or *group* dispersion curves; the difference between phase and

group depends on considering the velocity of one single wave (phase) or the envelope of more waves (group).

This work focuses mainly on the analysis of the methods used to estimate reliable surface wave dispersion curves in order to create a 3D surface wave tomography of Pacaya volcano. Our investigation of multiple tools which try to find these important velocity-frequency (and subsequent depth) relationships is not useful only for this particular volcano, but it can also be applicable to other active volcanic systems.

In the first chapter we introduce Pacaya volcano, Guatemala, and the data collected there for this study. In the chapter two, we describe the array of methods used to find the surface wave dispersion curves (group and/or phase) through the analysis of ambient noise. In chapter three we show the results, dividing those estimated using the Bensen et al. (2007) approach and the relative 1D shallow velocity model beneath the Pacaya volcano, and the results of comparison between the considered techniques, all based on the original idea of Aki (SPAC, 1957) but applied in unusual conditions. Then chapter four discusses all the results and, following the conclusion.

Chapter 1

Geology of Pacaya volcano

Pacaya volcano is a 2552 m high composite statovolcano located on the southern rim of the Pleistocene Amatitlán caldera, 30 km south of Guatemala City, Guatemala (14.381°N, 90.601°W) and it represents one of the edifices which forms the Guatemalan volcanic chain (WNW-ESE direction) (Fig. 1.1).

The entire volcanic complex includes the new composite cone ("Old Pacaya" and MacKenney cone), Cerro Grande, Cerro Chiquito and the Cerro Chino stratocones [5, 22, 29, 39, 69, 74]. All these eruptive centers, active during the Quaternary, have produced mainly porphyritic olivine/plagioclase-bearing basaltic lavas which no significant temporal chemical and petrographic variation [5, 11, 29, 38, 39]. Associated with these basaltic lavas, pyroxene andesites, dacites, rhyodacites and pyroclastic products have been erupted from the whole system [5, 21, 29].

The history of the Pacaya volcanic complex is not still clear, but Kitamura and Gómez [44] suggested that most of all Pacaya may be younger than 23 ka after the finding of extensive tephra over lied the Pinos Altos Fall deposit (dated 23 ka) in Pacaya region. In summary, at least four major eruptive phases have been recognized [5, 29] and they can be synthesized as:

- *Phase I*, characterized by the growth of an ancestral andesitic stratovolcano, subsequently eroded and covered by the Amatitlán caldera pyroclasts;

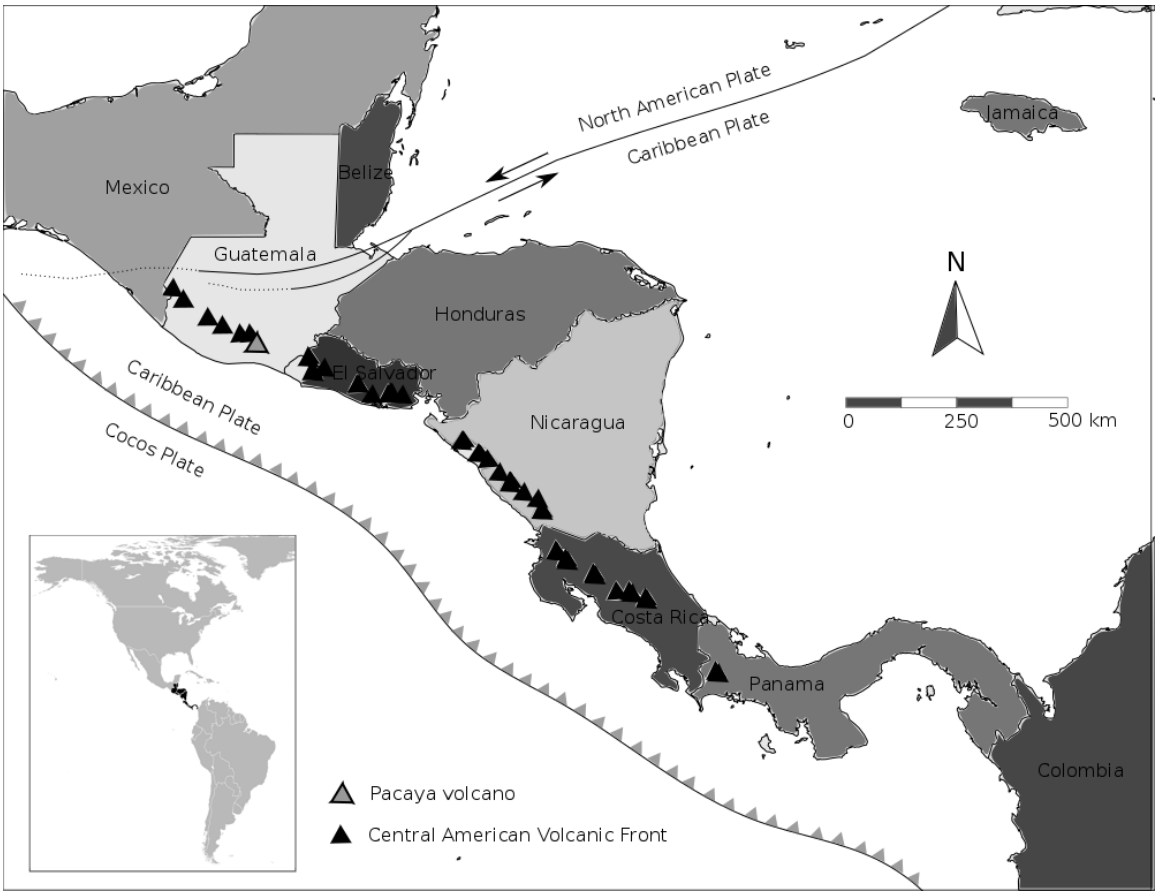

Figure 1.1: Map of the Central American Volcanic Front (CAVF). Pacaya volcano (Guatemala) is represented by the gray triangle, while the major part of the active volcanoes which form the CAVF are represented by black triangles.

- *Phase II*, dominated by a period of rhyodacite and andesite eruptions with the emplacement of the Cerro Grande and Cerro Chiquito stratocones;

- *Phase III*, where voluminous basaltic lava flows began to build the "Old Pacaya" stratocone. During this stage a sector collapse of the southwest side of the volcano occurred leaving a scarp visible nowadays. Starting in 1775 also the Cerro Chino stratocone become to form [69];

- *Phase IV*, characterized by the modern MacKenney cone building after the current active phase starting in 1961.

All these different stages represent only an interpretation of the complexity around the Pacaya volcanic system formation; the time between these phases described above is difficult to constrain, in particular because of the absence of abundant datable soils between eruptions and the lack of historical record before the 16th century [84]. Moreover, being the entire complex formed by several cones close to each other, the resulting volcanic stratigraphy is influenced by the contribute of all these eruptive centers yielding difficult the distinction.

The remarkable visible feature of the whole system is related to the large arcuate scarp which interests the "Old Pacaya" described by Eggers [29], within which the modern MacKenney cone is built. This scar was formed by a large (0.6-0.8 km^3) SW sector collapse triggering a debris avalanche that traveled 25 km down southwestward and laterally phreatic-phreatomagmatic explosions [44, 84]. Intepreted firstly as a caldera collapse fault [29, 30], evidence such as the similarity of composition between debris and lavas within the amphiteater and lack of correlation pyroclastic flow-tephra deposits suggest a gravitational collapse source [84]. It occurred approximately between 400 and 2000 yr B.P. [84], even though the work by Kitamura and Gómez [44] confined this event 600 and 1500 yr B.P. by tephra units dating. Although the activity of Pacaya records also short phases of moderate explosivity (rhyodacite and andesite products) with VEI up to 3, the dominant volcanism is certainly mafic [5, 11, 29, 69].

The modern MacKenney cone, grown after the 1965 eruption, is composed in fact by interbedded basaltic lavas and tephra [38, 39, 69]. An important feature regarding the activity at Pacaya volcano is that eruptive periods are episodic and not continuous, with large volumes of basaltic lavas and scoria erupted in 50-300 yr [84] and longer dormant intervals of about 300-500 yr [22, 62]. This behavior is reflected also by the recent volcanic stage begun with the eruption of about 1.5 x 10^6 m^3 in March 1961 after a period of more than 100 yr of quiescence [31].

Currently, the activity is characterized by persistent degassing [4] and alternates

between frequent strombolian events and aa lava flows extruding from the flanks of the MacKenney cone [23, 38, 67]. This apparently quiet effusivity is sometimes interupted by larger explosive eruptions such as the last one (VEI = 3) which occurred on 27 May 2010. Consequences of this relatively remarkable event were: significant topographic changes of the edifice including a linear collapse 600 m long oriented NNW from the summit; deposition of about 20 cm of ash and tephra in neighboring communities; the opening of a new vent on the SSE flank that produced a 5.4 km long lava flow; and about 3 m of co-eruptive movement of the SW flank measured through INSAR analysis [75]. The 2010 eruption is also important because it represents the first lava flow in modern period (after 1961) coming from a vent located outside the collapse amphiteater [39, 62], suggesting an active magmatic source not only confined in the recent MacKenney cone. Many authors agree that the geology and the eruptive behavior of Pacaya volcano indicate a presence of a mobile magma body at shallow depth [7, 29, 30, 31, 32, 38, 60, 68, 74, 75, 84, 89]. Eggers et al. [28] and Schaefer et al. [74] suggest that frequent microearthquakes, constant tremor [24], gravity changes at Pacaya, in additional to the structural features and discontinuities, could confirm shallow magma movement.

The Pacaya complex represents a unique volcano for event locations and structural setting. This volcano-tectonic relation, recognized in many volcanoes, plays in this case a key role in the understanding the behavior of this complex magmatic system.

1.1 Tectonic setting

Pacaya volcano is located in the middle part of the Guatemalan volcanic chain (see Fig. 1.1). This compressive environment is only one portion of the Central American Volcanic Front (CAVF) [11], which extends for about 1100 km from the Mexico-Guatemala border to Costa Rica and includes at least 40 major volcanic edifices [16]. The average spacing of eruptive centers in the CAVF is around 26 km [11, 14, 15] and it represents one of the highest volcano densities in subduction zone

settings [16]. This volcanic cluster WNW-ESE trending is the result of the subduction of the oceanic Cocos plate beneath the Caribbean plate [15, 55] with an angle of about 40° and variable convergence rate between 70 and 90 mm/yr southwards [25].

The magma composition range of these CAVF stratovolcanoes varies from basalt to dacite [11], even though the typical volcanism of arc is basaltic andesite and andesite. Gill [37] classifies the CAVF lavas as a medium K-andesites with calc-alkaline affinities.

The tectonic structure of the area surrounded Pacaya volcano is very complex and interesting, but it is not well studied (Fig. 1.2). Even though the geodynamics indicates a compressive regime (subduction), regionally the study area is located south of the active Montagua and Polochíc left-lateral transtensional fault zones accounting for the formation of many grabens including Guatemala City Graben (GCG), which absorbs most of the E-W extensional deformation estimated of about 8 mm/yr [10, 36, 40, 54]. This movement and the extensional tectonics down the Montagua and the Jocotán faults has accompanied rotation of the trailing edge of the Carribbean plate around these faults [10].

Moreover, this area is split by the WNW-striking right-lateral strike-slip Jalpatagua fault zone (JFZ) and Pacaya volcano is situated at or near the intersection of the GCG and JFZ [11, 74, 90]. Right in this intersection is located the Pleistocene Amatitlán caldera, formed between about 300 ka B.P. to less than 23 ka B.P., and the entire Pacaya volcanic complex lies on the southern rim of it [90].

Although the trace of the JFZ is not defined, topographic maps suggest that Pacaya edifice is probably intersected by this system of faults (Fig. 1.2). There are two possible confirmations of this hypothesis:

- Historical and recent vents are aligned about NNW-SSE parallel to the JFZ. This suggests that the volcanic rift zone (VRZ) coincides with the direction of the Jalpatagua fault system. The NNW-SSE alignment identifies the orientation of the regional horizontal greatest principal stress (σ_{Hmax}) and it is

perpendicular to the least principal stress (regional σ_3);

- Pacaya volcano was subjected by a sector collapse around 0.6-1.5 ka B.P. oriented about SW producing a debris avalanche (about 0.65 km^3) that traveled 25 km SW of the edifice [44, 84]. Many studies [45, 63, 78, 79, 82, 83] indicate that edifice collapses are favorable orthogonally to the VRZ (volcanic σ_1), that in this case is oriented about NNW-SSE. Therefore, the ancestral and future sector collapses of the SW flank could be coherent with this idea [74]. As a demonstration, recent work of Schaefer et al. [75] demonstrated that the last eruption of Pacaya in May 2010 triggered a landslide, visible with INSAR data, always toward the SW flank of the volcano.

The alignment of the active MacKenney vent, Cerro Chino and the 2010 opened vent outside the ancestral scarp seems to validate the NNW-trending volcanic rift of Pacaya and this geometry may be certainly influenced by the regional stress field. In particular, the combination of the strike component of the JFZ and the extensional GCG may have a key effect on the Pacaya structure and its eruptive behavior.

Finally, collapses and landslides toward SSW have already happened in Pacaya's history and they may repeat in the future.

1.2 Data acquisition

During the January 2015 (14-21) field campaign, a seismic network of 19 short-period seismometers was deployed around Pacaya vent with distances between stations from about 300 to 2500 km (Fig. 1.3). We used Mark Products/Sercel 3-component L-22 sensors with a natural frequency of 2 Hz and a sensitivity of 88 V/m/s. Data were recorded on 12 Reftek 130 digitizers operating in continuous mode at 125 samples per second and equipped with Global Positioning Systems (GPS) timing. Station locations were determined independently with GPS.

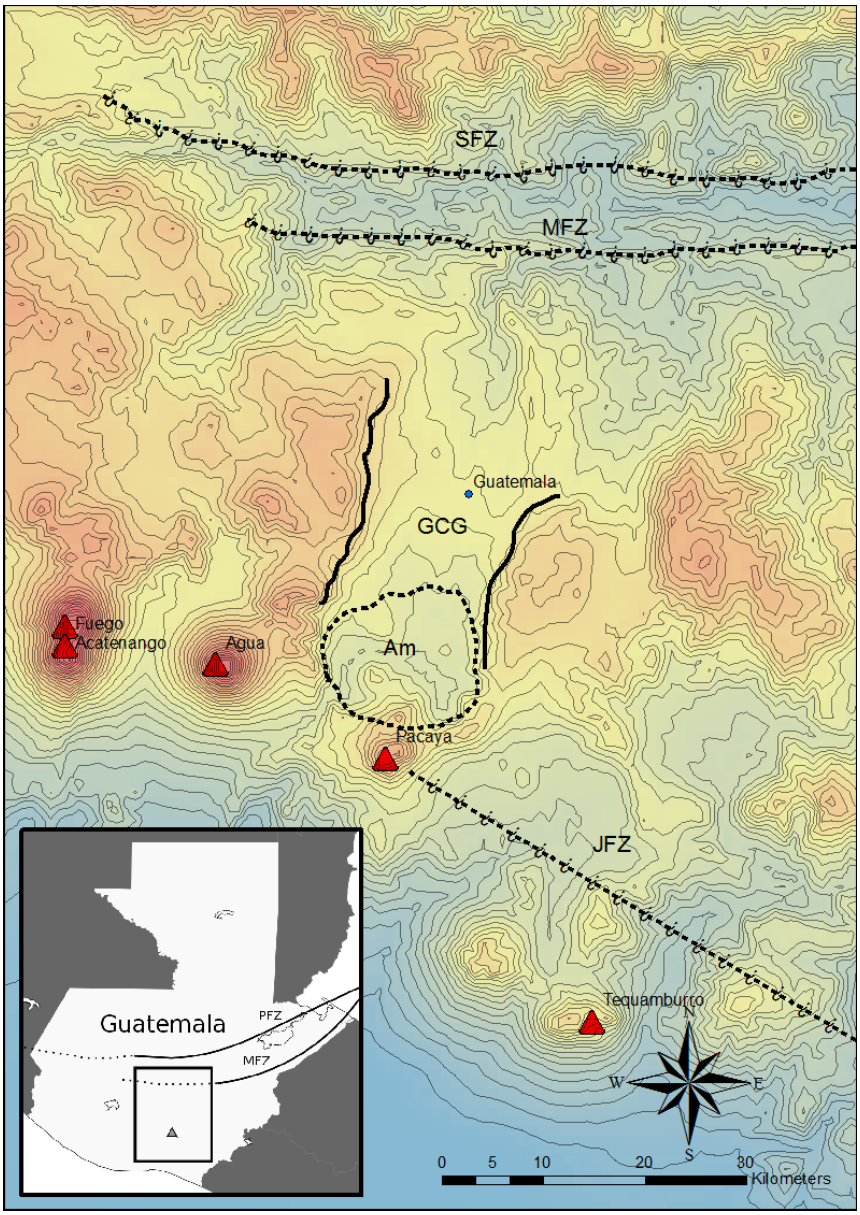

Figure 1.2: DEM of area around Pacaya volcano (orange triangle). Other Guatemalan volcanoes are represented in red triangles. With black lines are sketched the major tectonic structures: *Am* = Amatitlán caldera; *GCG* = Guatemala City graben; *JFZ* = Jalpatagua fault zone (right-lateral strike-slip fault); *MFZ* = Montagua fault zone (left-lateral transtensional fault); *PFZ* = Polochíc fault zone (left-lateral transtensional fault); *SFZ* = San Augustine fault zone (left-lateral transtensional fault). Dashed line indicates uncertainty in the fault trace, while dashed lines with question marks represent inferred fault traces.

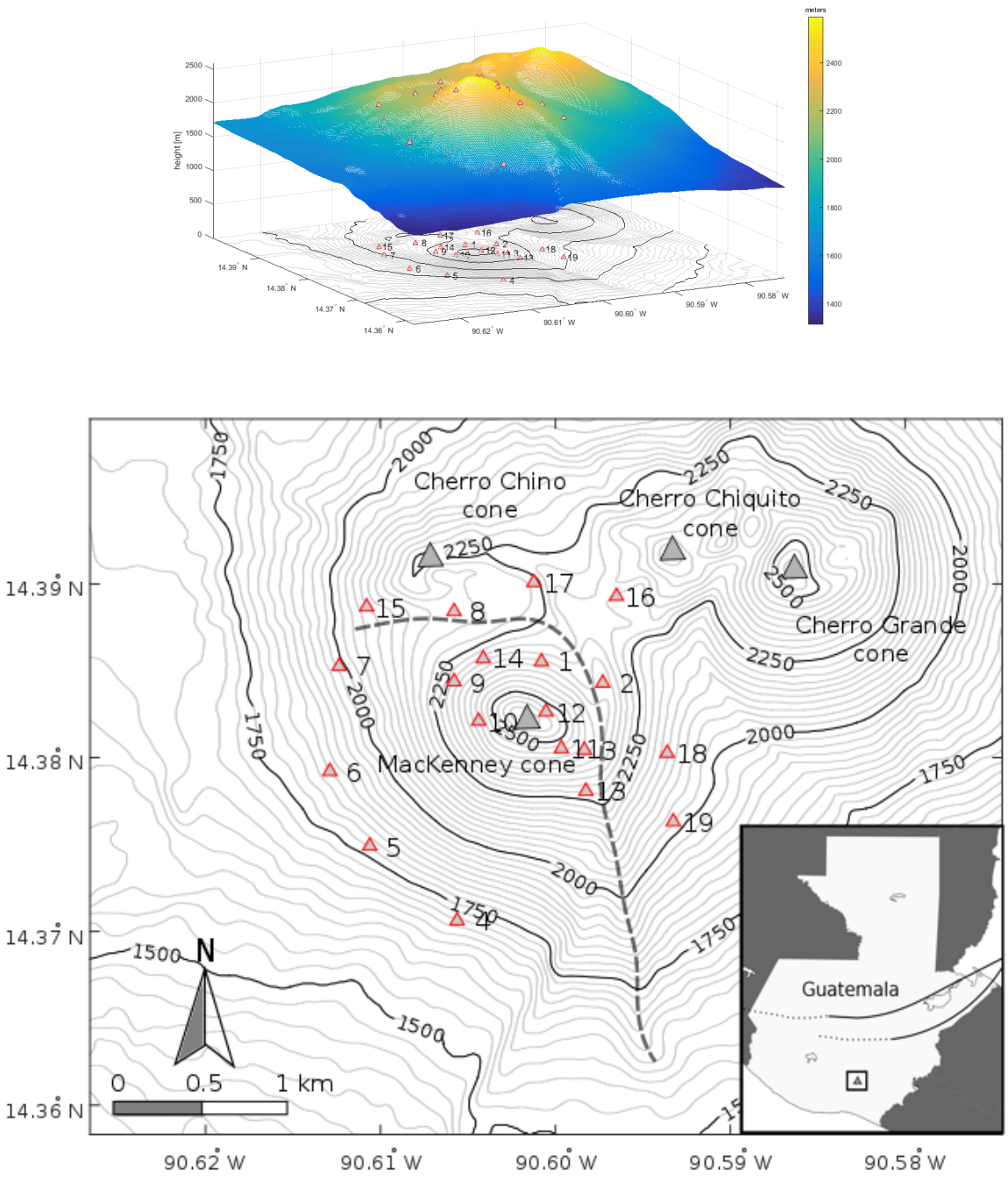

Figure 1.3: Temporary stations location (red triangles) during the 14-21 January 2015 field survey at Pacaya volcano, Guatemala. The grey dashed line represents the scarp collapse. All stations inside this scar are related to the new MacKenney cone (*New Pacaya*), while those in the convex part are deployed in the ancestral Pacaya (*Old Pacaya*). With grey triangles are indicated the location of the other cones forming the entire Pacaya complex.

Chapter 2

Ambient noise analysis

Ambient noise surface wave analysis is a rapidly advancing technique that uses ambient noise correlation to reconstruct surface waves propagating between stations. Aki [1] and more recent studies have demonstrated that the result of the cross-correlation of ambient noise between two or an array of seismic stations represents the Green function (Earth response) beneath the stations [1, 2, 3, 6, 26, 48, 80, 85, 86, 87, 88]. The original idea supposes that this ambient noise is principally dominated by surface waves, Rayleigh and Love [12, 13, 64, 71, 72, 76]. All of the approaches to derive Green functions from ambient noise rely on correlations between data from pairs of stations, which may performed in either the time or frequency domain. The differences come from how the cross correlations are interpreted. The following sections describe the methods used in this study.

2.1 Bensen et al. (2007) analysis

To isolate ambient noise in a seismogram, Bensen et al. [6] described a general processing to obtain reliable broad-band surface wave dispersion measurements, including temporal normalization (one-bit, running-absolute mean, water-level,...) and spectral whitening in order to remove earthquakes and other signals. The hourly

cross-correlation between a pair of stations can be done in the time and frequency domain. Temporal stacking is the next step, in order to decrease the noise and increase the SNR (Signal-Noise Ratio) [13, 47, 76, 77, 92].

After the data processing, the goal is to estimate the dispersion curves (group and phase velocities) to find the surface wave velocity as a function of frequency. This is a very important step and it represents a crucial part to create a 1D and 3D ambient noise tomography. To do this, Bensen et al. [6] suggest to use the so-called *Frequency-Time ANalysis (FTAN)* [27, 42, 49, 50, 51, 52, 66, 70], basing on the definition of velocity and the idea of a random isotropic wave-field [86].

In a random isotropic wave-field, if some components of the noise are coherent at two stations (it can be thought as a wave starting from the first station and propagating to the second station), the time delay between this arrival at the two stations can tell us the velocity structure between the stations, that is the Green function. This approach consists to calculate the velocity (group and phase) as a ratio of the distance between the two stations and the lag time of the peak in the cross-correlation (made in the time-domain).

These methods are considered valid only if the number of analyzed days to do the cross-correlation is large enough to increase the SNR and the distance between stations is greater than two-three wavelengths, because time-domain studies depend on the far-field approximation in the interpretation of the Green function [53, 77, 91, 92];

2.2 SPAC (Aki, 1957)

SPAC (SPatial AutoCorrelation method) is introduced for the first time by Aki [1], and developed by other authors as Ferrazzini et al. [35], Chouet et al. [19], Metáxian et al. [59], Chouet et al. [20] and Saccorotti et al. [73]. The general assumption is based essentially on two hypothesis of the wave-field [1]:

- Ambient vibration (wave-field) is stochastic, isotropic and stationary in both time and space. In simple words, the wave-field is randomly distributed, it does not change as a function of time and space and its physical properties are the same regardless of orientation;

- The wave-field consists of dispersive surface waves, that is it is composed by surface waves with different frequencies which travel with different velocities.

As a consequence, the autocorrelation function (correlation coefficient, that is how the waveforms recorded by two different stations are similar to each other) of the wave-field is related to the phase velocity curve through a Bessel function (eq. 2.1, see Appendix A for details). In other words, the result of the cross-correlation (they use cross-correlation in the time-domain, but it is also possible in the frequency-domain) between a pair of stations can be seen as a Bessel function of the zero order J_0, whose argument is the ratio between the angular frequency times the distance and the phase velocity:

$$\overline{\rho}(r, \omega_0) = A J_0 \left[\frac{\omega_0}{c(\omega_0)} r \right] \tag{2.1}$$

where $\overline{\rho}(r, \omega_0)$ is the correlation coefficient, that is the result of the cross-correlation between a pair of stations separated by distance r, A is generally equal to 1, ω_0 is the angular frequency ($= 2\pi f$) where f is the frequency and $c(\omega_0)$ is the phase velocity as a function of frequency.

This idea of the similarity between the cross-correlation between a pair of station and a Bessel function is the key thing on which other authors started to develop other methods to find phase dispersion curves. For instance, Ferrazzini et al. [35], Chouet et al. [20], Saccorotti et al. [73] and Lanza et al. [46] applied the idea of Aki to small aperture seismic arrays in different volcanoes with inter-station distances up to 500-600 m finding the shallow 1D velocity model beneath each array.

Moreover, they suggested that the formula of Aki (eq. 2.1) can be also used not only in vertical-vertical (ZZ) cross-correlation to find the Rayleigh dispersion curve

as Aki did, but also in the radial and tangential components to find the Love wave dispersion curve and the component of the Rayleigh wave in the radial component, simply using the Bessel function of first order J_1 and a ε value.

In particular, they calculated the phase velocity dispersion curves considering the zero-crossings, maxima and minima of the correlation coefficient and they fitted it using power-law curves of the type of eq. 2.2. The equation on the left was proposed by Saccorotti et al. [73], whereas that on the right by Chouet et al. [20]:

$$c(f) = Af^{-b} \qquad\qquad c(f) = Af^{-b}e^{-cf} \tag{2.2}$$

where f is the frequency and A, b and c are constants, estimated using a least-squares error grid search [73]. The use of zero-crossings, maxima and minima of observed cross-correlation derives from the similarity of this to a seismic wave, characterized by a wavelength equals to the inter-station spacing. So, at $1/4\lambda$ there is a zero-crossing, at $1/2\lambda$ we have a minimum, at $3/4\lambda$ another zero-crossing, then at 1λ there is a maximum and so on.

2.2.1 Ekström et al. (2009) and Haney et al. (2012) methods

Ekström et al. [34] developed a simple technique to estimate phase velocity measurements from the zero-crossings of the cross-correlation in the frequency-domain (correlation spectrum). The idea, based on the suggestions of Aki [1], consists that the cross-correlation in the time and frequency domains can be thought as a Bessel function, whose argument is the ratio of the product between the angular frequency ω and the distance r between two stations and as a denominator the phase velocity curve $c(\omega_n)$. Therefore, the phase velocity at each zero-crossing can be calculated using eq. 2.3.

$$c(\omega_n) = \frac{\omega_n r}{z_n} \tag{2.3}$$

where z_n denotes the nth zero of the Bessel function of the zero order, J_0.

Haney et al. [41], starting from the idea of Aki [1] of isotropic and stochastic wave-field and the work of Ekström et al. [34], suggested that in order to increase the number of zero-crossings we can use not only the vertical-vertical (ZZ) cross-correlation between a pair of stations, but also the vertical-radial (ZR), because in the vertical and the radial components only Rayleigh waves propagate. The estimation of the phase velocity dispersion curve for the vertical-radial (ZR) cross-correlation is made using the zeroth of the Bessel function of the first order, J_1. The advantage of these methods is that they can be applied even in those conditions where the distance between stations is smaller than one wavelength [33, 34].

2.2.2 Chávez-García et al. (2005) method

Basing on the formula of Aki (eq. 2.1), there are other methods that are used to estimate the surface wave dispersion curves. For instance, Chávez-García et al. [17] propose to use the inversion method (eq. 2.4 [57]) in order to find the best phase dispersion curve from the result of the cross-correlation between a pair of stations, where, as guess for the inversion problem, they suggest to use the formula of Saccorotti et al. [73] (eq. 2.2).

$$d_0 = g(p) \tag{2.4}$$

where d_0 represent the data parameters that in our case are the autocorrelation functions, $\overline{\rho}(r, \omega_0)$, p are the model parameters and in our case they coincide with the argument of the Bessel function in eq. 2.1, while g is the matrix which links the data to the model parameters and in our case is the Bessel function of the zero order, J_0. Indeed, the formulation and the process is more complex and it is described in detail in the paper of Chávez-García [17].

2.2.3 Menke and Jin (2015) method

Finally, a further method is proposed by Menke and Jin [58] in which they divide the dispersion curve process essentially into two steps, basing on the idea that phase velocities tends to vary smoothly with frequency:

- *Grid search for initial estimate of the solution*, which starts fixing the upper and the lower bounds of phase velocity and defining three or more frequency nodes at which the phase velocity is specified and the number of values that it can take at each node. The next step is linearly interpolating the velocities at all nodes. They choose the linear interpolation because the phase velocity tends to vary smoothly with frequency. The grid search is done to find the best phase velocity of every node in order that the Bessel function of zero order in eq. 2.1 of the dispersion curve is similar to the correlation coefficient. The amplitude A in the formula of Aki is not a parameter that can vary in the grid search because it can be computed by least squares once phase velocities are specified (eq. 2.5):

$$A = \frac{\left[\rho^{pre}(c, A=1)\right]^T \rho^{obs}}{\left[\rho^{pre}(c, A=1)\right]^T \rho^{pre}(c, A=1)} \tag{2.5}$$

  where ρ^{pre} is the correlation coefficient (= result of the cross-correlation between a pair of stations), ρ^{obs} represents the result of the Bessel function of zero order calculating from the grid search of the phase velocities at each node, c is the phase dispersion curve obtained from the grid search (including the linearly interpolated phase velocities);

- *Solution refinement by Generalized Least Squares*, uses the estimate just found in the first part smoothing it through the inverse problem [57] of the type of eq. 2.6 and similar to the eq. 2.4:

$$\Delta d = G\Delta m \tag{2.6}$$

where Δd is the variation of the data parameters, G is the matrix linking the data parameters to the model parameters and Δm is the change in the model parameters.

Chapter 3

Data processing and results

To create a seismic velocity model from ambient noise, the most important step is finding the phase or group velocity curves. We have seen that there are different techniques to estimate them, but almost all of them are valid and they can be applicable only if the distance between pairs of stations is greater than two-three wavelengths [53, 77, 91, 92], or they require a small aperture array with a typical configuration (see [20, 46, 73]). Another important requirement is that a lot of data be used to improve the signal. All techniques, except the analysis with a small aperture array, are typically applied only if the available number of days to study is in the order of one month or more [6, 8, 9, 17, 18, 34, 41, 53, 56, 58, 65, 76, 91]. The explanation why we need a lot of days to analyze involves the level of noise affecting the data; in particular Bensen et al. [6] indicate that greater is the number of available days, greater is the Signal-Noise Ratio (SNR) and it is important mainly in the cross-correlation. In fact, if we consider the idea of Weaver [86], only one wave or few waves in a random isotropic wave-field can be assumed as the result of a wave originated in a station and propagating toward the second station. As a consequence, the signal of this wave can be detected in the cross-correlation of this pair of stations. Obviously, if the level of noise is high, the signal of this wave can be easily confused with noise and so it becomes more difficult to identify the signals in the cross-correlation.

After deconvolving the instrument response from the 8 available days we applied

all the methods described above. For this purpose we used only the vertical component (in the SPAC we used vertical, north and east channels), therefore we analyze only Rayleigh waves.

Our goal is to try to apply these methods in our case at Pacaya volcano, dominated by *small distances between stations* (less than two wavelengths) and *few days of data* (4-7 days), to see whether these techniques can be used in common conditions (temporary stations and relative small edifice) in a active volcano as Pacaya. Firstly, we describe the Bensen processing and the result of 1D shallow velocity model, followed by the analysis of the data and the relative results using all other techniques based on the original idea of Aki (SPAC, 1957).

3.1 Bensen et al. (2007) approach

As Bensen et al. [6] describe in their paper, we have normalized the data using the one-bit normalization (we have tried to use also the running-absolute mean normalization, but the results are not so different from each others), removing the mean, high-pass filter 1-10 Hz and finally we normalize the spectra using a spectral whitening as described by Bensen (Fig. 3.1).

This process was done for all 19 stations. A hourly cross-correlation in the time-domain was made for all pairs of stations and the results were stacked for all the available days (Fig. 3.2). An important thing is that not all stations recorded the same days, so the number of analyzed days in which it was possible to do the cross-correlation become reduced to 4-7 days (see Appendix B).

In order to find the dispersion curves, in particular the group velocities, we filtered from 0.5 to 3.5 Hz with 0.5 Hz long windows, made the envelope and estimated the lag time (highest peak in the cross-correlation). Assuming valid the idea of Weaver [86], we calculated the group velocity simply dividing the distance between a pair of stations by the lag time. The level of noise was large enough to have group dispersion curves with some peaks, but for many frequencies the value of the group velocity was

reasonable as we could expect in a volcano (the values were comparable with other works done in a volcano, as Brenguier et al. [9] at Piton de la Fournaise). This is more probably due to the small number of days in the cross-correlation (as we expected) and the SNR was not so high.

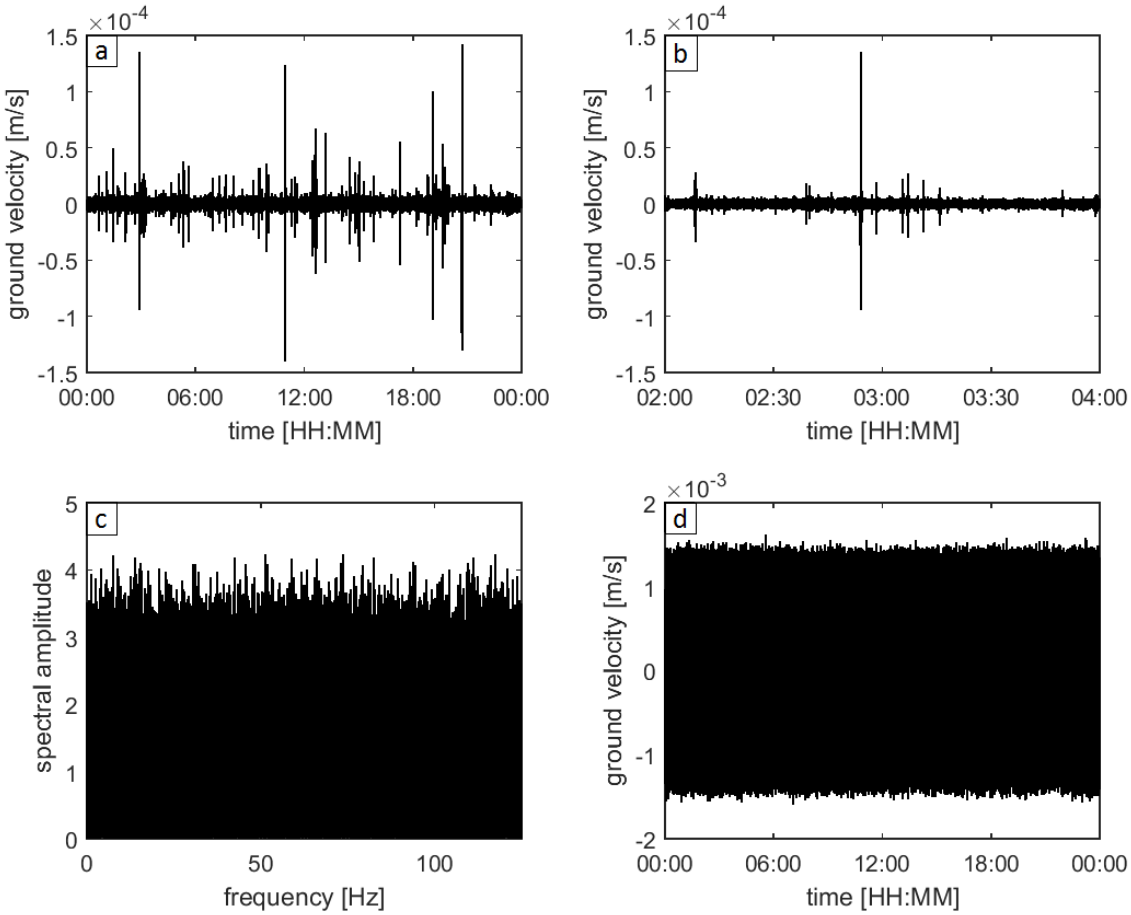

Figure 3.1: Example of data processing for one day (15 January 2015) at station *PS04* as described by Bensen et al. [6]. *a*) deconvolved data by the instrument response of the entire day (15 January 2015); *b*) zoom on two hours of deconvolved data; *c*) spectral whitened amplitude spectra for 125 samples per second of the all analyzed day; *d*) all day normalized data (in time and frequency domain) used in the cross-correlation.

To solve this problem, we removed manually the spikes and considered only those frequencies for which the value of group velocity was reasonable. A curiosity consists

that we noted that above 1.5-2 Hz many dispersion curves showed a rise (Fig. 3.3). Not trusting all our dispersion curves we tried to create only a 1D velocity model beneath Pacaya volcano, discarding the idea of a 3D velocity model for the inconsistency of the group velocity curve for every pair of stations.

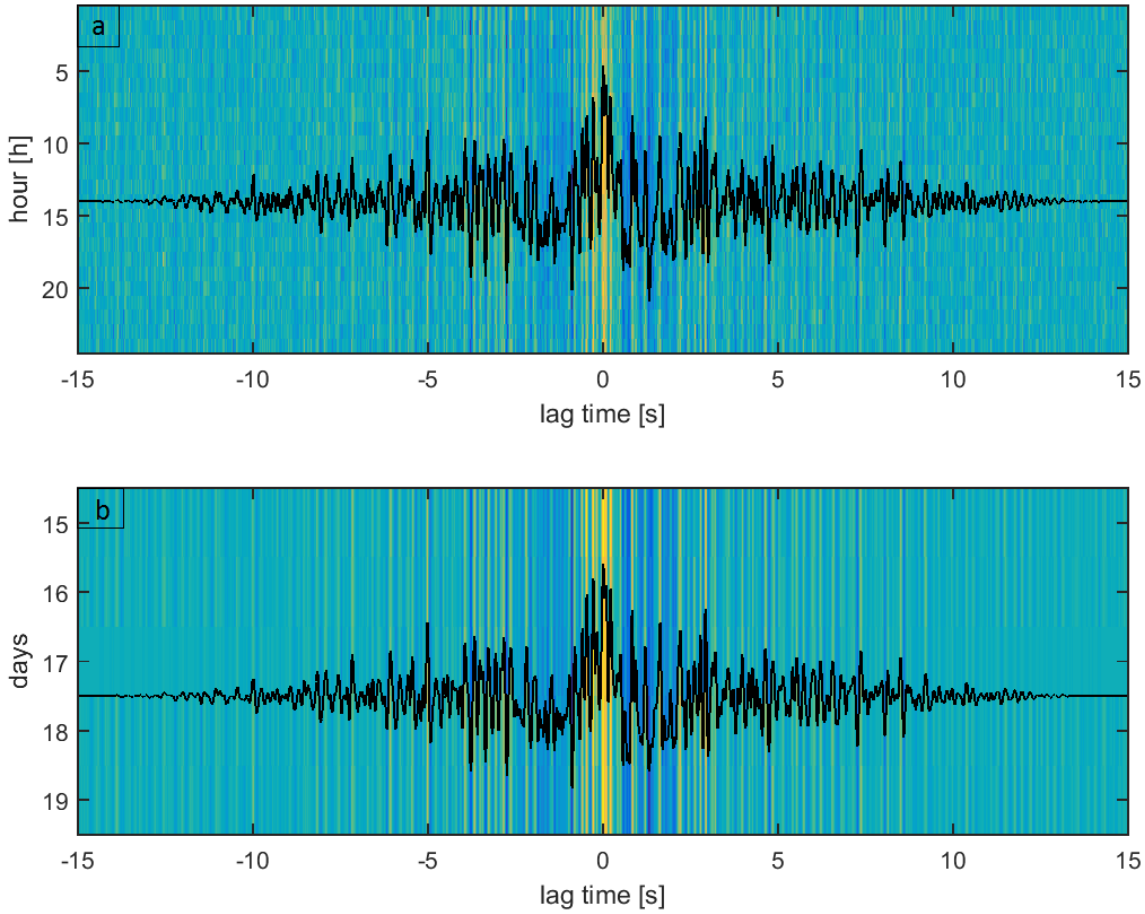

Figure 3.2: Example of cross-correlation in time-domain between stations *PS07* and *PS15*. *a*) background: hourly cross-correlation of 17 January 2015; the seismogram represents the stacked signal of the entire day. *b*) background: daily cross-correlation between the two stations from January 15 to 19; seismogram is the stacking for all overlapping days.

Knowing the complexity of the structure of Pacaya, in particular the scar due to the ancestral sector collapse, we tried to separate the results of the cross-correlation for the stations located in the old part of Pacaya (in the ancestral edifice) and in the

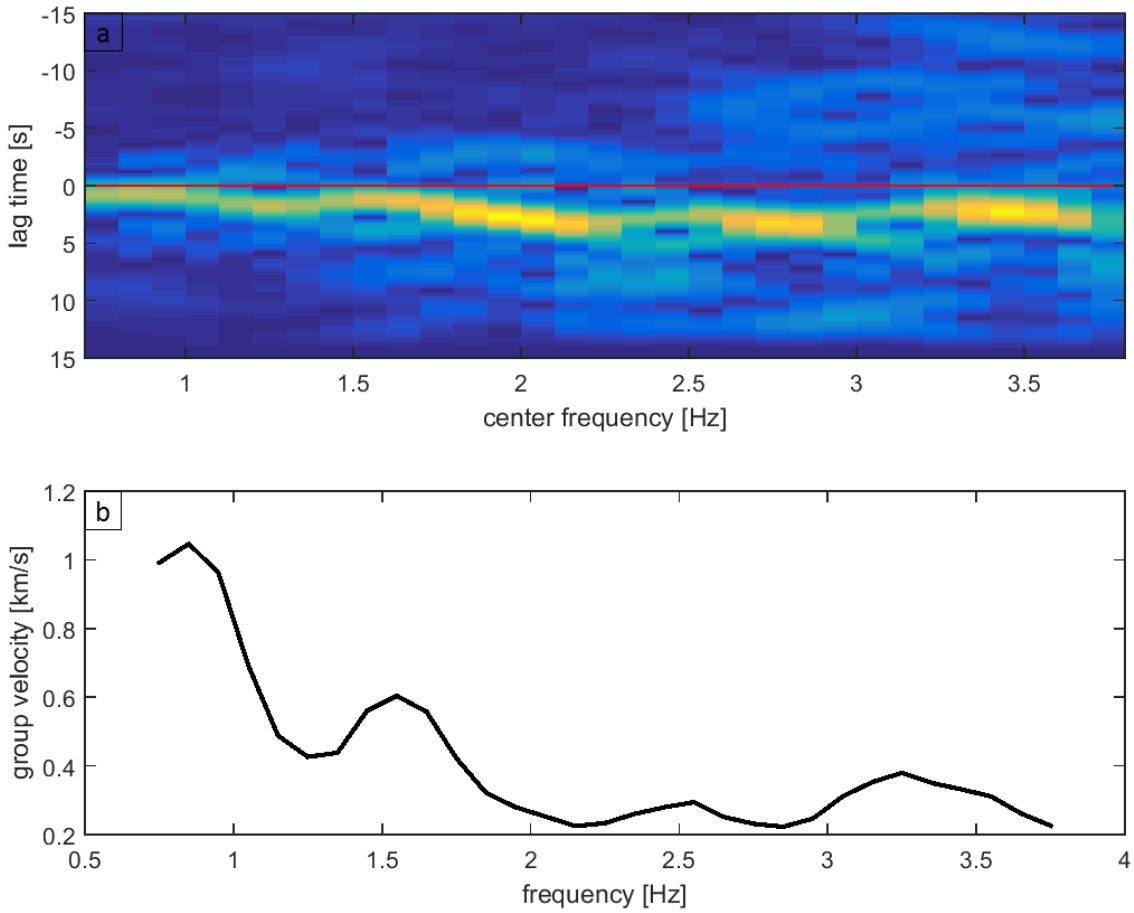

Figure 3.3: Example of group velocity estimation using the definition of group velocity between stations *PS08* and *PS10*. *a*) envelope of the waves as definition of group surface waves for each frequency. *b*) group dispersion curve where the group velocity for each frequency is calculated in the peak in the envelope (yellowish color) in *a*). Red line represents the 0 s lag time.

new MacKenney cone (built after the collapse) (see Fig. 1.3 and Tab. 3.1). Under the assumption that the dispersion curves represent the fundamental modes of Rayleigh waves, we performed an iterative 1D inversion of these curves ([43]; the procedure is described in detail in that paper) to derive a shallow shear-wave velocity model beneath the array (Fig. 3.4, Fig. 3.5 and Fig. 3.6). Our result was compared with the shallow 1D velocity model of Pacaya made by Lanza et al. [46], found using the same approach of Chouet et al. [20], Ferrazzini et al. [35] and Saccorotti et al. [73]

with a small aperture array deployed in the SW flank during the field campaign in 2011.

Table 3.1
Division of stations based on their location respect to the old edifice (*Old Pacaya*) or in the new MacKenney cone (*New Pacaya*).

Edifice	**Stations**
Old Pacaya	PS08-PS15-PS16-PS17-PS18-PS19
New Pacaya	PS01-PS03-PS04-PS05-PS06-PS07-PS09-PS10-PS11-PS12-PS14

With the approach of Bensen et al. [6], we can calculate mainly Rayleigh group velocity curves. To improve the result we decided to add the phase dispersion measurements obtained using the Ekström technique [34]. The cross-correlation between a pair of stations was made in the frequency-domain and the phase velocity was calculated using the zero-crossings of the zero-order Bessel function (eq. 2.3). For the same reason of the Bensen method, the SNR was pretty low so we could estimate only the first two-three zero-crossings of each cross-correlation (Fig. 3.7).

The result, shown in Tab. 3.2, 3.3 and 3.4 and Fig. 3.8, cannot be considered very reliable, because the few days of data (4-7 days) decrease the SNR, but it appears clearly that from old Pacaya and new Pacaya there is not evidence of large differences in the velocity structure and, moreover, this result is not so different respect to the 1D shallow velocity model estimated by Lanza et al. [46] and it can be compared to it. Probably if we would have more days of data, some differences in the old Pacaya and in the new part would appear, because we expect that the new Pacaya might be "warmer" than the old side, so the velocity should be lower than the old edifice.

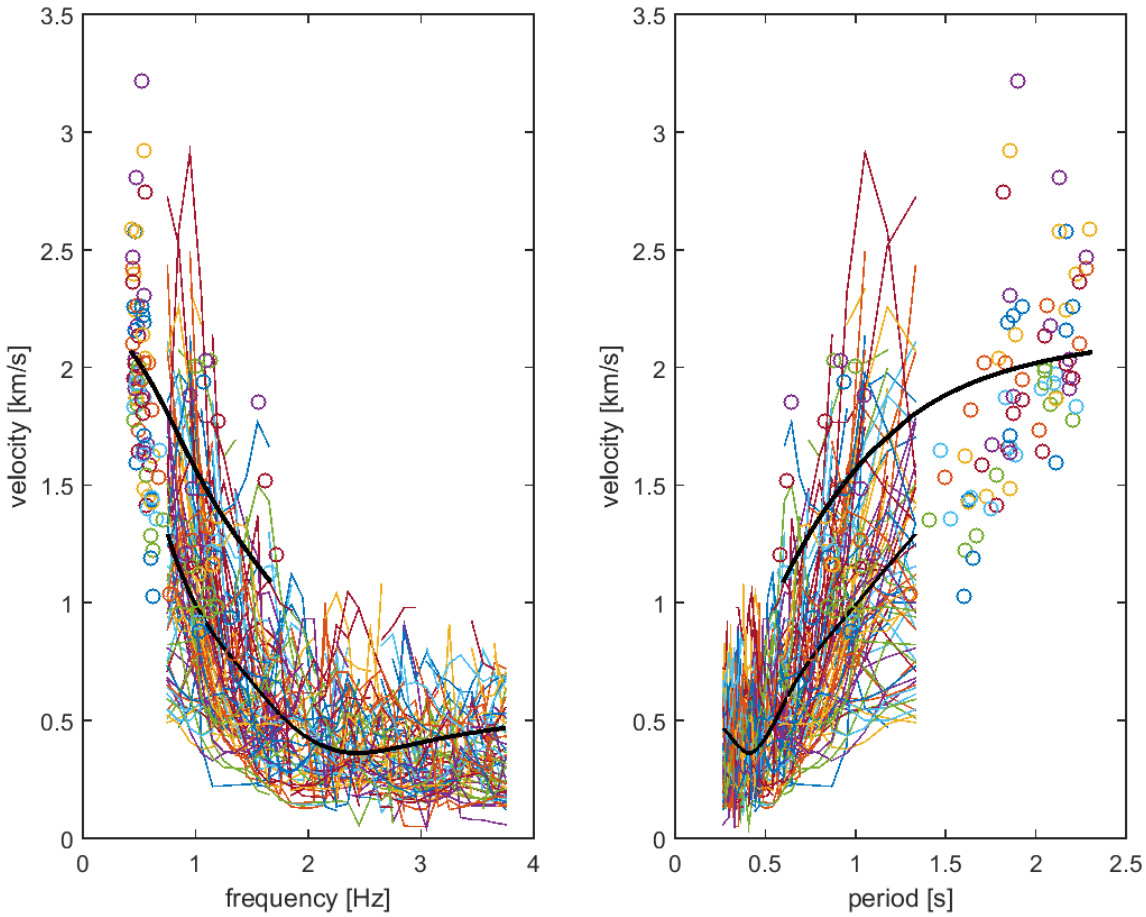

Figure 3.4: Group and phase dispersion curves (two black lines) for ***All Pacaya*** used in the iterative 1D inversion [43]. In colored lines are represented the dispersion curves (or segments of them) for all pairs of stations, while in colored circles are represented phase velocities obtained using the Ekström method. In the two panels are represented group and phase velocity as a function of frequency (left) and period (right).

Table 3.2
1D shallow velocity model of ***All Pacaya***, that is considering all stations.

Thickness (km)	v_P **(km/s)**	v_S **(km/s)**	**Density (g/cm^3)**
0.1000	1.0239	0.5912	2.1174
0.1500	2.0478	1.1823	2.3582
0.3500	3.5264	2.0360	2.2304

Table 3.2 – continued

Thickness (km)	v_P (km/s)	v_S (km/s)	Density (g/cm^3)
0.5000	3.9400	2.2903	2.3212
0.0000	4.3326	2.5015	2.3830
Tot 1.1000			

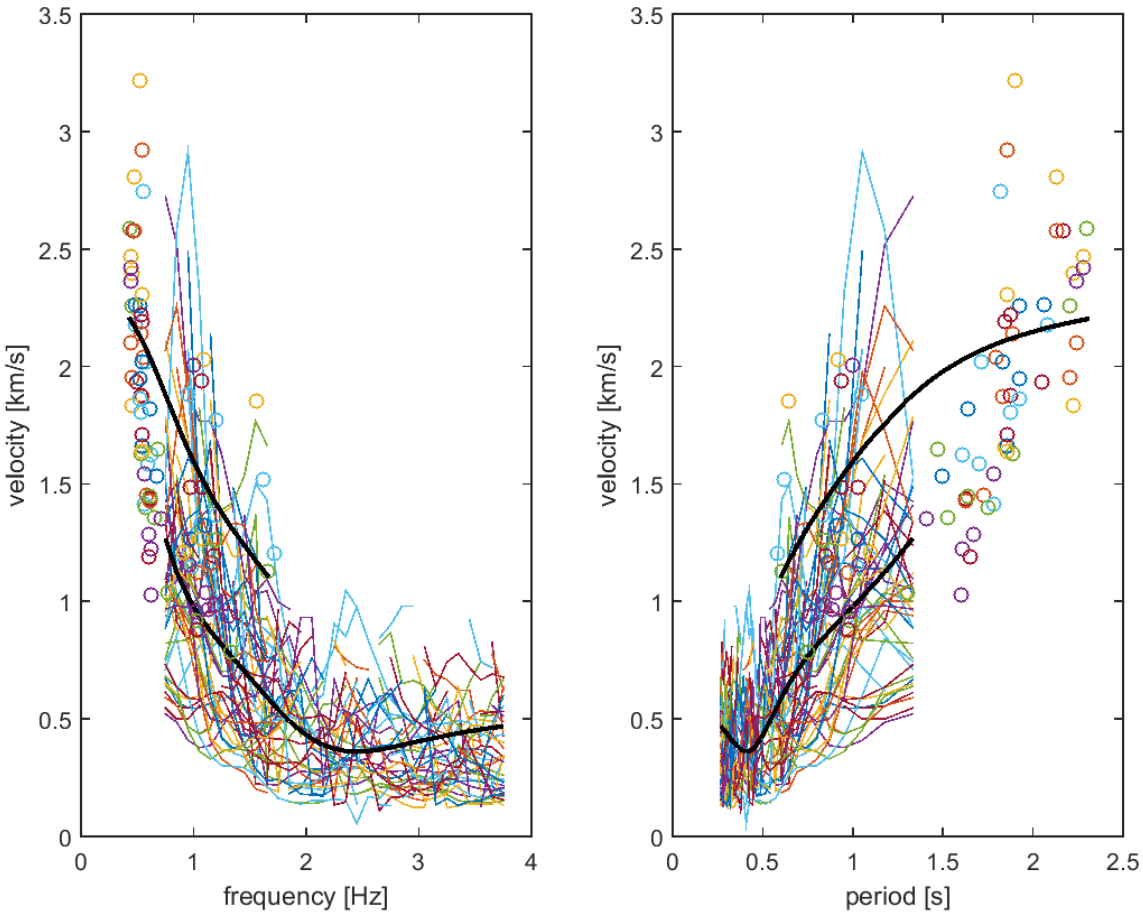

Figure 3.5: Similar plot as Fig. 3.4 for ***Old Pacaya***.

Table 3.3
1D shallow velocity model of ***Old Pacaya***, that is considering all stations.

Thickness (km)	v_P **(km/s)**	v_S **(km/s)**	**Density (g/cm^3)**
0.1000	1.0140	0.5855	2.1140
0.1500	2.0398	1.1777	2.3568
0.3500	3.5022	2.0220	2.2281
0.5000	4.0085	2.3301	2.3362
0.0000	4.4502	2.5694	2.4274
Tot 1.1000			

Table 3.4
1D shallow velocity model of ***New Pacaya***, that is considering all stations.

Thickness (km)	v_P **(km/s)**	v_S **(km/s)**	**Density (g/cm^3)**
0.1000	1.0277	0.5934	2.1187
0.1500	2.0784	1.2000	2.3633
0.3500	3.5230	2.0340	2.2452
0.5000	3.9818	2.3146	2.3549
0.0000	4.6647	2.6932	2.4981
Tot 1.1000			

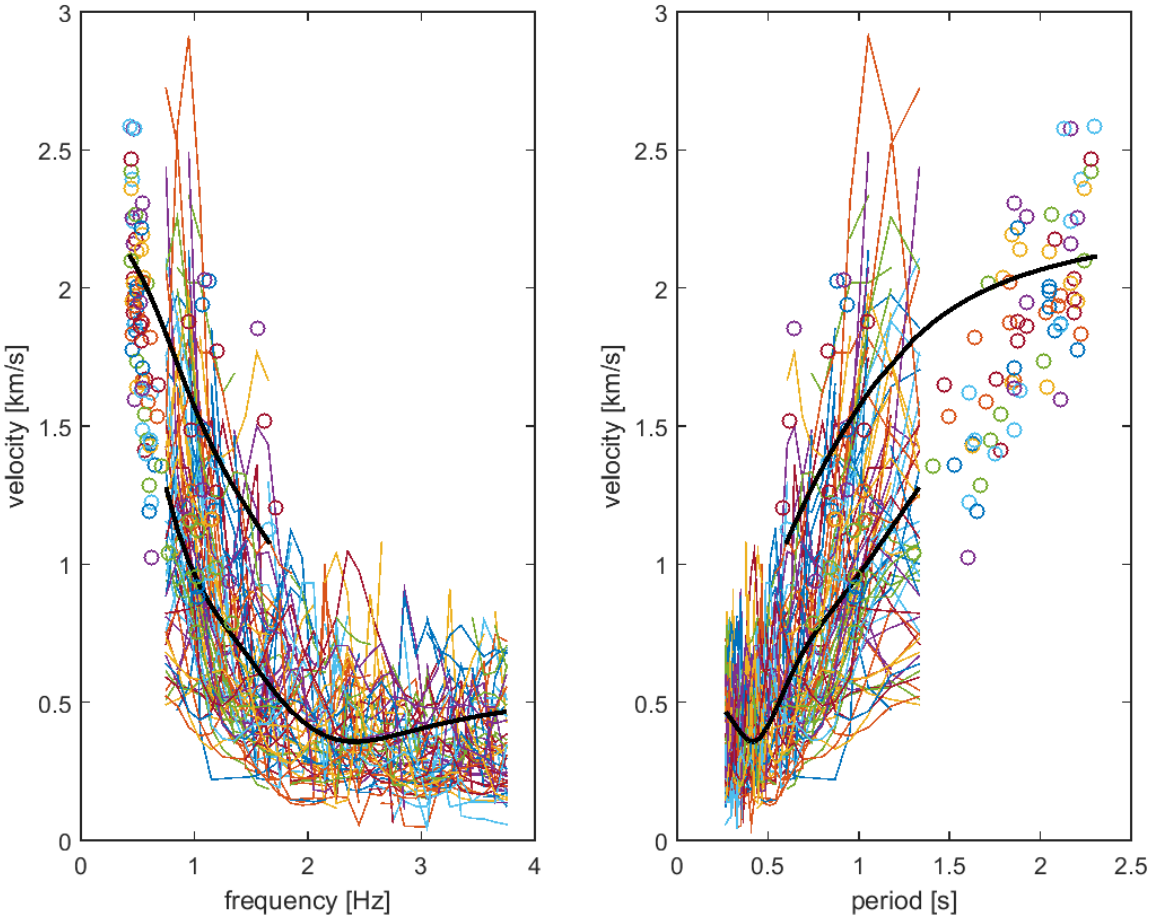

Figure 3.6: Similar plot as Fig. 3.4 for ***New Pacaya***.

3.2 SPAC approach

The idea of the SPAC method [1] is applied in many techniques which tried to estimate the surface wave dispersion curves, but the use of this approach in active volcanoes is rare and it is applied only to a small aperture array [20, 35, 46, 59, 61, 73, 81] and, as a consequence, it is useful only to build a 1D velocity model of the subsurface beneath the array (that is a small portion of the edifice). It has never been applied to an entire volcano and built a 3D velocity model of the all edifice.

Our goal is trying to use the SPAC method to create a 3D ambient noise tomography of Pacaya volcano. The first step, as described in detail in the paper of Saccorotti

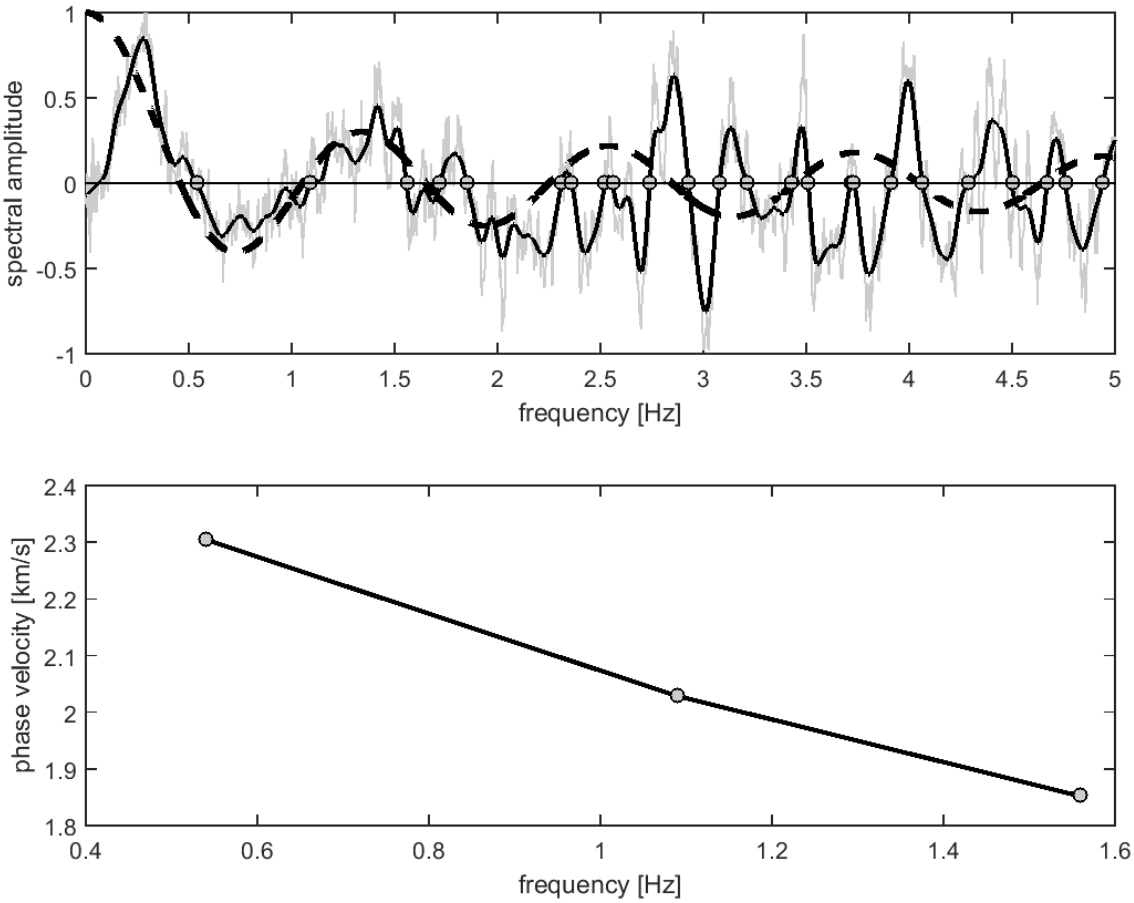

Figure 3.7: Example of phase dispersion curve found using the Ekström et al. [34] method for station *PS09-PS19*. In the top panel is represented the cross-correlation in frequency-domain (grey line); the black solid line indicate the smoothing of the spectral amplitude, while the black dashed line is the Bessel function of the cross-correlation calculated using the formula of Aki [1].

et al. [73], is selecting time windows of many minutes in which there are no events and all signal is dominated by ambient noise. Saccorotti et al. [73] chose 6-9 windows of 3 minutes long, while Lanza et al. [46] used 16 of 5 minutes long. We have found 139 time windows of 24-360 seconds in which Pacaya showed only noise (tremor) (see Appendix C). The correlation and summing procedure (stacking) was conducted for all frequencies from 0.25-10.20 Hz with 0.1 Hz steps.

The main difference respect to the classic method is that we considered only a pair

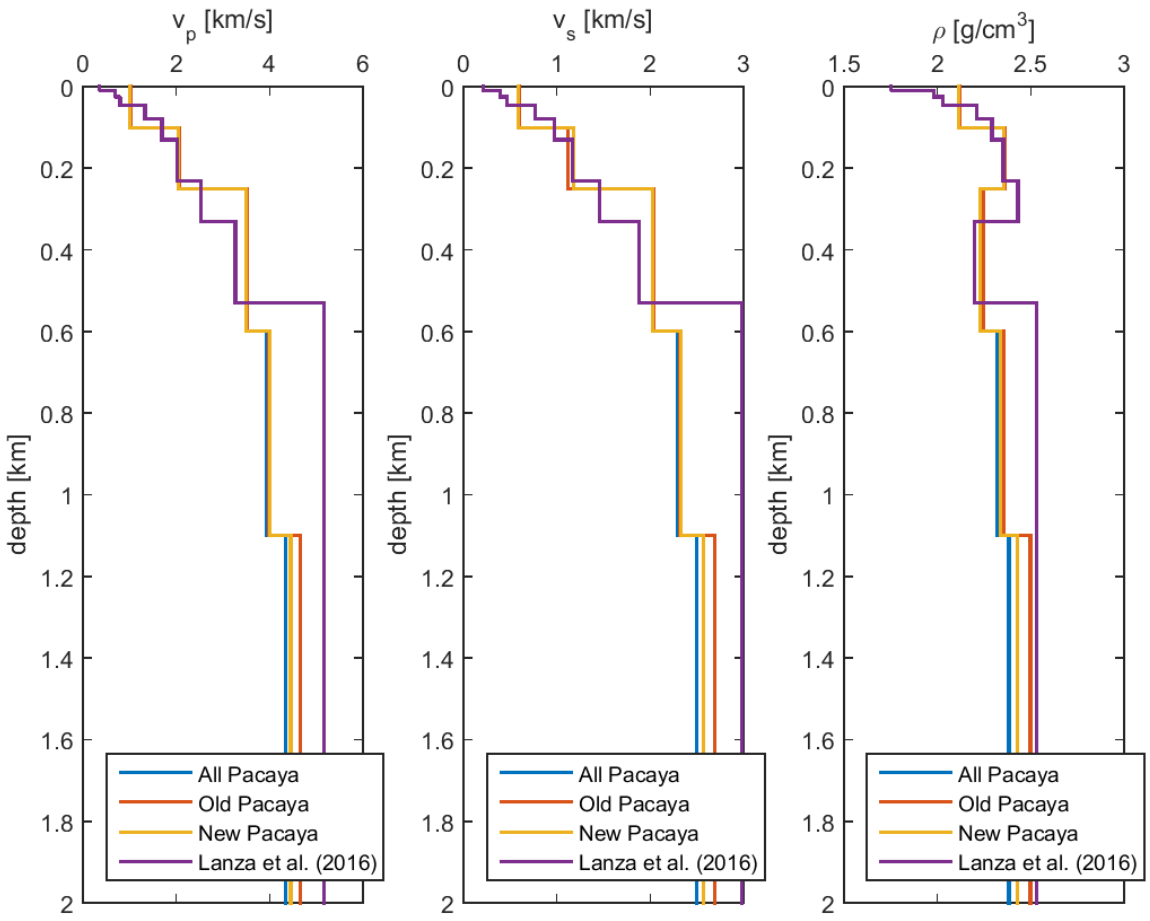

Figure 3.8: 1D shallow velocity model (up to 1.1 km) of Pacaya found using the inversion approach of Herrmann et al. [43]. The blue line represents the result for ***All Pacaya***; the orange line for ***Old Pacaya*** and the yellow one for ***New Pacaya***. The purple line represents the 1D shallow velocity model (up to about 600 m) obtained by Lanza et al. [46] from a small aperture array in 2011.

of stations and not a seismic array. Considering a small aperture array instead of only two stations, the SNR increases because the number of analyzed stations increases, so we can take only a small number of time windows in the cross-correlation because that number must be multiplied by the number of stations at the same distances. To avoid this problem and increase the value of SNR, we decided to consider only a pair of stations but increasing the number of time windows and, as a consequence, the number of cross-correlations increases. Then we stacked all these cross-correlations

of 139 time windows to obtain the autocorrelation function $\overline{\rho}(r, \omega_0)$ (eq. 2.1). We considered reasonable and valid only results of the cross-correlation between 0.5 and 3 Hz (Fig. 3.9).

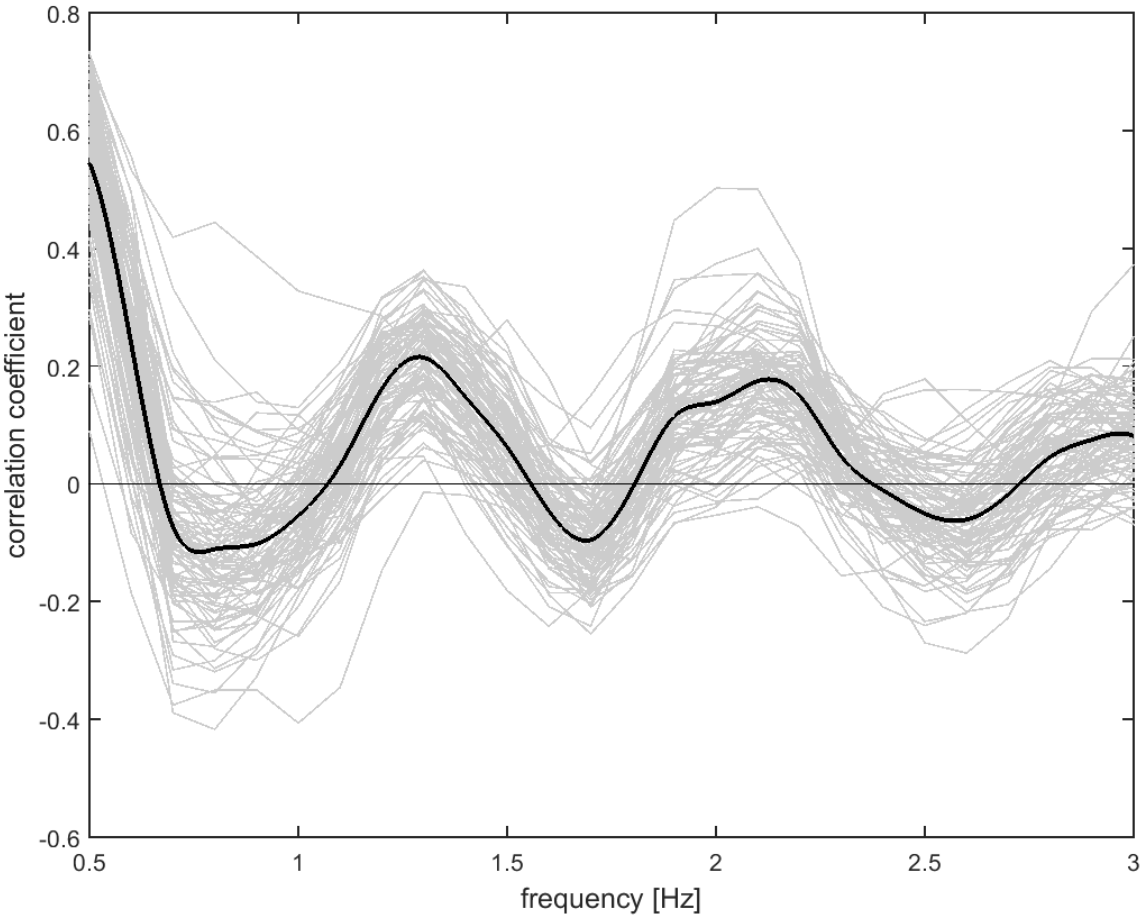

Figure 3.9: Example of vertical-vertical (ZZ) cross-correlation between stations *PS05* and *PS09*, 1.29 km apart (look at the map (Fig. 1.3) for their location). The grey lines represent the results of the cross-correlations of the 139 selected time windows, while the black solid line indicates the stacked line (simply the mean), in order to increase the SNR.

The lower bound was chosen for two reasons: firstly we used short-period seismometers with natural frequency of 2 Hz and, secondly, the distance between stations varies about 300-2200 meters suggesting that we are not able to trust waves characterized by long periods (= long wavelengths). The upper bound was chosen because

being in a volcano, we expect that high frequencies are more subjected to scattering and attenuation than lower frequencies and we have seen that above about 3 Hz the correlation coefficient become too different respect to a Bessel function.

From the Fig. 3.9 it appears clear that almost all cross-correlations of the time windows follow the same trend and increasing the number of time intervals increases the SNR, such as the number of days in the Bensen et al. [6] procedure. Moreover, all of them seem to describe a Bessel function similar to that theorized by Aki [1]. Following the procedure described by Chouet et al. [20] and Saccorotti et al. [73], we estimated the phase dispersion curves considering zero-crossings, maxima and minima and we used the following formula:

$$c_R(f) = f(n)r\frac{4}{n} \qquad \text{where } \lambda = r\frac{4}{n} \tag{3.1}$$

where n is the number of zero-crossings, maxima and minima. The idea of this formula is based on the classic formula that connects velocity to frequency and wavelength ($v(f) = f\lambda$). The correlation coefficient (similar to a Bessel function) can be thought as a wave. Therefore, the first zero-crossing is located at 1/4 of the wavelength; the minimum at half wavelength; the second zero-crossing at 3/4 and the maximum at 1 wavelength and so on.

After calculating the dispersion curve (using the right formula of eq. 2.2), the checking wheter this curve is reasonable consists to use the formula of Aki (eq. 2.1) in order to estimate the calculated autocorrelation function and compare it with the observed one (= our result of the cross-correlation). The result, shown in Fig. 3.10, approximates the Rayleigh dispersion curve as a power law and this curve is used to build the calculated autocorrelation function (represented with the black dashed line in the right panel), while the observed one is represented with the solid line. We can see that the velocity of the first zero-crossing probably is too high to be a surface wave velocity in a volcanic area. In fact, also the Bessel function is not perfect.

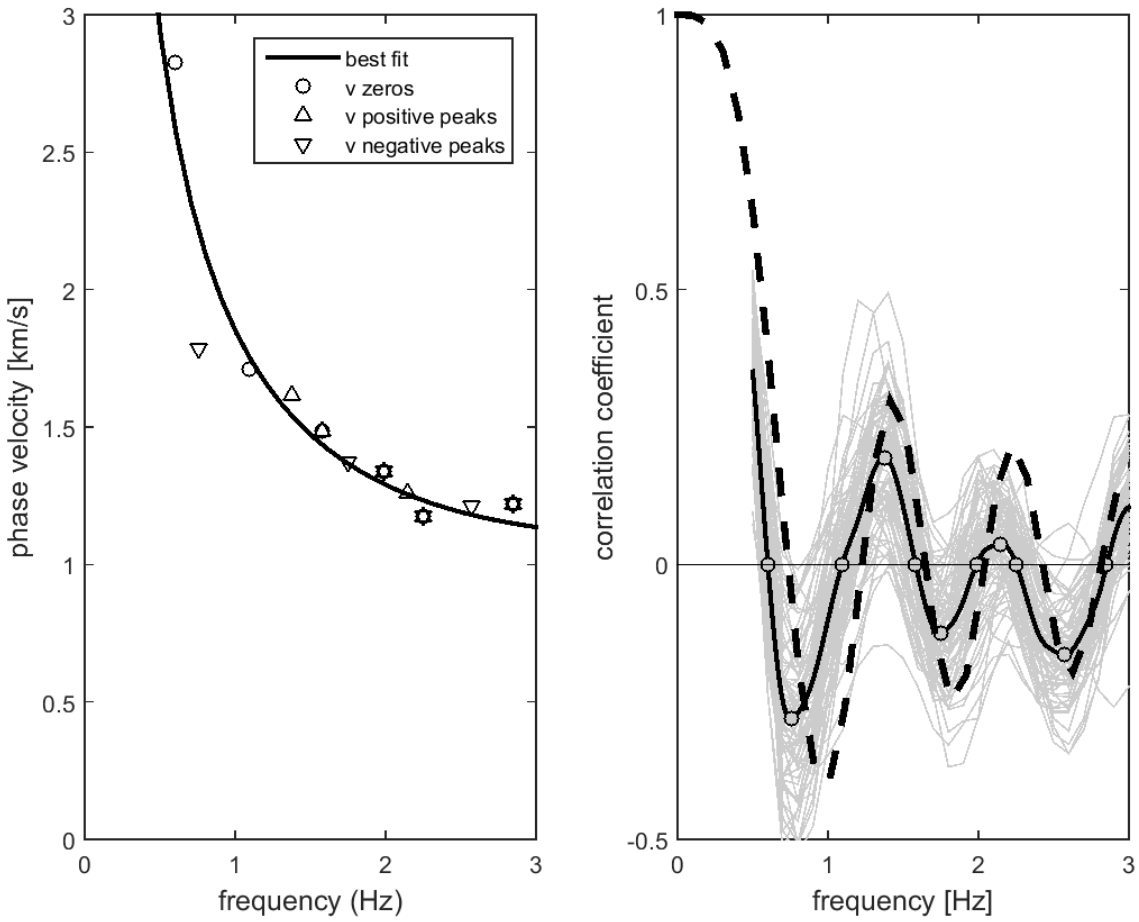

Figure 3.10: Example of phase dispersion curve between stations *PS10* and *PS16* (left), 1.18 km apart. The black solid line is the best fit (eq. 2.2) of the velocities of zero-crossings, maxima and minima calculated with eq. 3.1. On the right panel, the grey lines represent the results of the cross-correlations of the 139 selected time windows, while the black solid line indicates the stacked line (simply the mean), in order to increase the SNR. The dashed black line represents the calculated correlation coefficient from the phase dispersion curve estimated in the left panel.

We found 26 phase dispersion curves whose the result of the cross-correlation looked like a Bessel function without correcting missed or extra zero-crossings. We were not satisfied from these results for three reasons:

- No perfect matching between the observed and calculated autocorrelation function, resulting presumably from the simplistic formula fitting the velocities considering zero-crossings, maxima and minima. These formulas (Chouet et al. [20] and Saccorotti et al. [73]) might be used to fit data from a small aperture array, but considering only a pair of stations they are not probably the best fits;

- Velocities probably too high for being in a active volcanic system. These found Rayleigh phase velocities are higher respect to those calculated beneath a small aperture array at Pacaya by Lanza et al. [46]. Looking at other works of ambient noise tomography such as Brenguier et al. [9] at Montserrat volcano, they found group velocities considerably smaller;

- Phase velocities seem to be rapidly decreased up to 1-1.5 Hz becoming quite flat after this threshold.

3.2.1 Chávez-García et al. technique

The next step was trying to apply another method to find the dispersion curves without using the formulas of eq. 2.2. We used the method proposed by Chávez-García [17]. This procedure, described above and in detail in their paper, is based on a inverse problem. Rather than starting with a grid search (forward problem), they suggest to start with an estimate of the dispersion curve and modify it through many iterations until the calculated autocorrelation function becomes similar to that observed one.

This approach is very interesting because it is not based on equations, but it assumes valid the original idea of the SPAC [1] and the process reaches the results through decreasing RMS (Root-Mean-Square error). We tried to apply this method following the procedure described in Chávez-García [17] paper, but the results did not converge to a solution.

3.2.2 Menke and Jin method

A further recent method that we tried to apply was proposed by Menke and Jin [58]. This can be divided into two parts: am initial grid search to estimate the dispersion curve, and an inverse problem similar to that of Chávez-García [17]. For our purpose we focused only on the grid search, because it is simpler and it represents the first step to check if this procedure is valid.

We, first, selected the upper and the lower bounds in which the phase velocities are likely to be. We chose 0.1-3.0 km/s; after this, we computed the grid search of only three nodes (frequencies) and 40 iterations for each node calculating the Bessel function using the Aki's formula (eq. 2.1) to estimate the calculated autocorrelation function and comparing it with the observed one.

We found 26 phase dispersion curves in which it was possible to overlap the phase velocities estimated with the zero-crossings (Ekström [34] method applied to SPAC-type short window correlations) and the Menke and Jin [58] approach. An example is represented in Fig. 3.11. It appears clear that the two different techniques overlap very well and the calculated correlation coefficient also fits well the observed autocorrelation function. This suggests that these two methods, even though we only used the first part of the Menke-Jin method, can be used to calculate the phase dispersion curve assuming the original equation of Aki is valid (eq. 2.1). Moreover these two methods can be applied not only for a small aperture array, but also for analyzing pairs of stations separated by 200-300 meters to about 1.3-1.5 km and probably more. We can also noted that, with respect to the previous method (SPAC of Chouet et al. [20] and Saccorotti et al. [73]), the approach of Menke-Jin includes the Bessel function amplitude (eq. 2.5) resulting in a better fits with the observed cross-correlation data (look at the right panel of Fig. 3.10 and the left panel of Fig. 3.11). Even with this procedure we can recognize the same issues obtained with the previous method, that is high velocities and fairly flat at frequencies above 1-1.5 Hz.

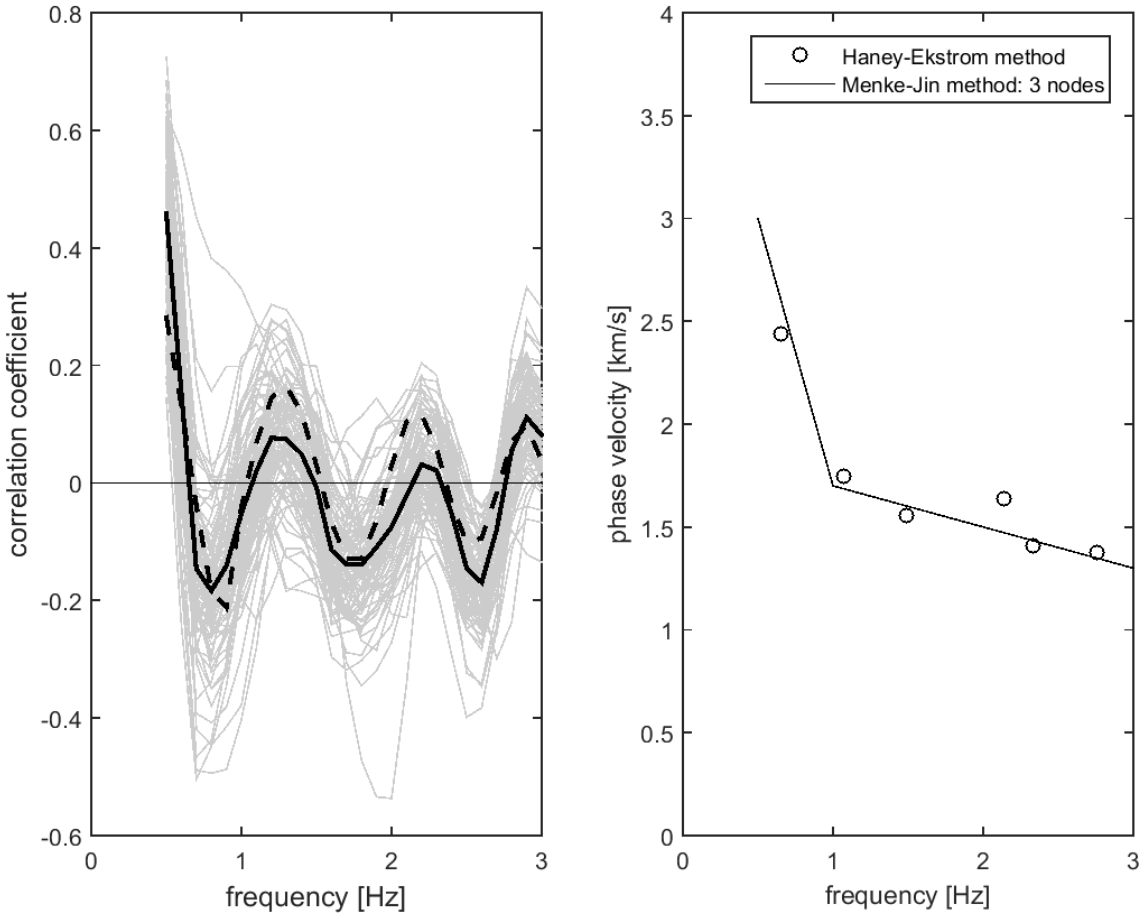

Figure 3.11: Example of phase dispersion curve between stations *PS07* and *PS12*, 1.44 km apart, estimated using the Ekström method and the Menke-Jin method (right). The black solid line is the curve obtained from the grid search of 3 nodes (*Step I*) suggested by Menke and Jin [58], while the black open circles are the velocities of the zero-crossings proposed by Ekström et al. [34].

3.2.3 Haney et al. technique

Finally, we used the Haney et al. [41] approach. This technique, based on the idea of Ekström et al. [34] and ultimately on Aki's [1] work, is usually applied to the result of cross-correlation in the frequency-domain, but we wanted to apply it to the SPAC-type short window correlations, following the SPAC approach of Chouet et al. [20] and Saccorotti et al. [73]. This idea to use this tool in a different context was

proved by the fact that the Menke-Jin method fit the zero-crossings calculated using the Ekström formula quite well (see Fig. 3.11). So, we applied the same formulation to the vertical-radial (ZR) cross-correlation and radial-vertical (RZ) one, except using the zeros of the Bessel function of the first order, J_1. Since Rayleigh waves propagate in the vertical-radial plane, these correlations might better constrain the Rayleigh wave phase velocities. An example of the result is shown in Fig. 3.12.

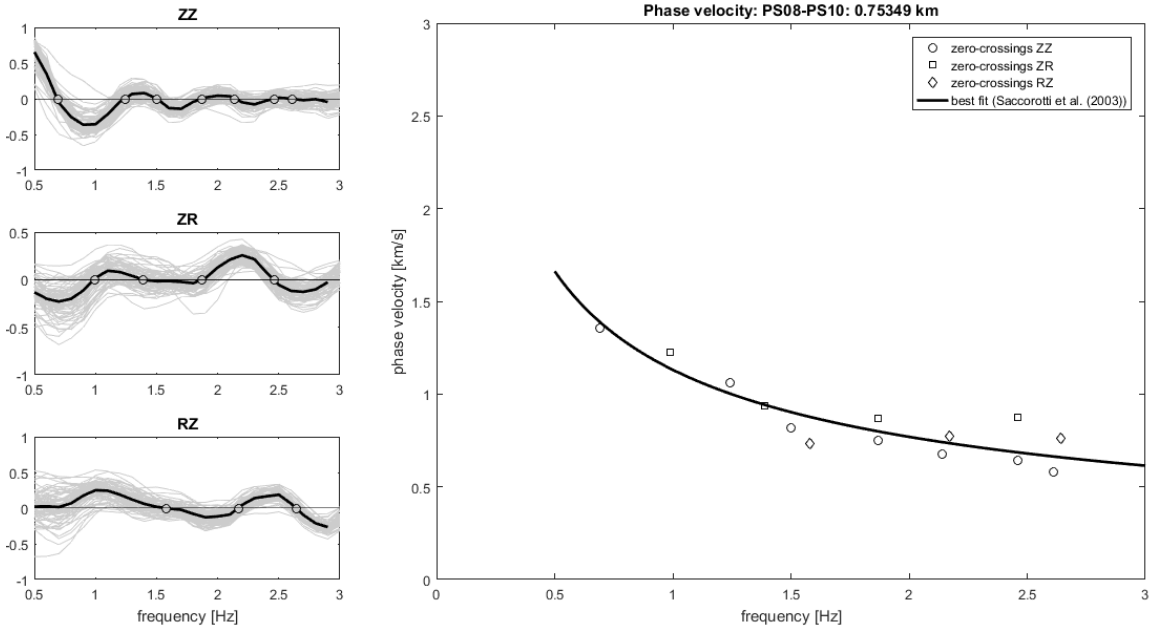

Figure 3.12: Example of phase dispersion curve between stations *PS08* and *PS10*, 753.5 m apart, estimated using the Haney et al. [41] method. The solid line is the curve obtained from the least-squares error grid search of Saccorotti et al. [73] (eq. 2.2). Black open circles are the phase velocities calculated using the zero-crossings of the vertical-vertical (ZZ) cross-correlation [34], while black open squares are velocities obtained using zero-crossings of vertical-radial (ZR) cross-correlation and the black diamonds of radial-vertical (RZ).

The main problem of these methods that fit zero-crossings involves the assumption that the result of the cross-correlation should look like a Bessel function [1]; as described by Ekström et al. [34] the association between a given zero with a zero-crossing of the Bessel function might be difficult due to the noise causing missed or

extra zero-crossings. The identification of these missed or extra zero-crossings may be difficult and not completely objective; therefore the resulting phase velocities are subjected to corrections with respect to their automatic calculations.

We found that only 26 vertical-vertical (ZZ) cross-correlations are not affected by missed or extra zero-crossings, while if we consider all three cross-correlations (ZZ, ZR and RZ), it is practically impossible to find perfect "Bessel functions" for all three components (see Appendix D). In the example of Fig. 3.12 we corrected two missed zero-crossings in the radial-vertical cross-correlation (RZ). Keeping in mind this issue, we fit these phase velocities using a power-law equation (following a least-squares grid search based on the formula of Saccorotti et al. [73] in eq. 2.2). We used this approach for 66 dispersion curves. For some of them the velocities calculated from the zero-crossings fit the power-law (Fig. 3.12), whereas for others the result of the corrected zero-crossings do not align very well with the fitting. The reason might be related to the lack of objectivity in the identification of the missed and extra zero-crossings.

3.2.4 Comparison between methods

We have tried different methods to estimate the phase velocity dispersion curves beneath an active volcano as Pacaya in Guatemala. All of them, except the Bensen et al. [6] approach, are based on the original idea of Aki [1] of stochastic wave-field and we used all of these techniques starting with the selection and the cross-correlation (between a pair of stations) in the time domain of a large number of time windows (139) of 24-360 seconds long, also for the Ekström et al. [34] and Haney et al. [41] techniques.

Our curiosity motivated the comparison of these different techniques in order to underline whether these give comparable results or they differ a lot from each other. For this purpose, never done before in literature, we decided to analyze different pairs of stations characterized by different distances in order to show the variability

of these approaches in different conditions. We have a range of distances between stations that varies from 300 meters to about 2.3 km; we did not consider stations more than 1.5 km apart, because the noise was too high and the observed correlation coefficient becomes more and more different from a Bessel function. Four examples are shown in Fig. 3.13, Fig. 3.14, Fig. 3.15 and Fig. 3.16.

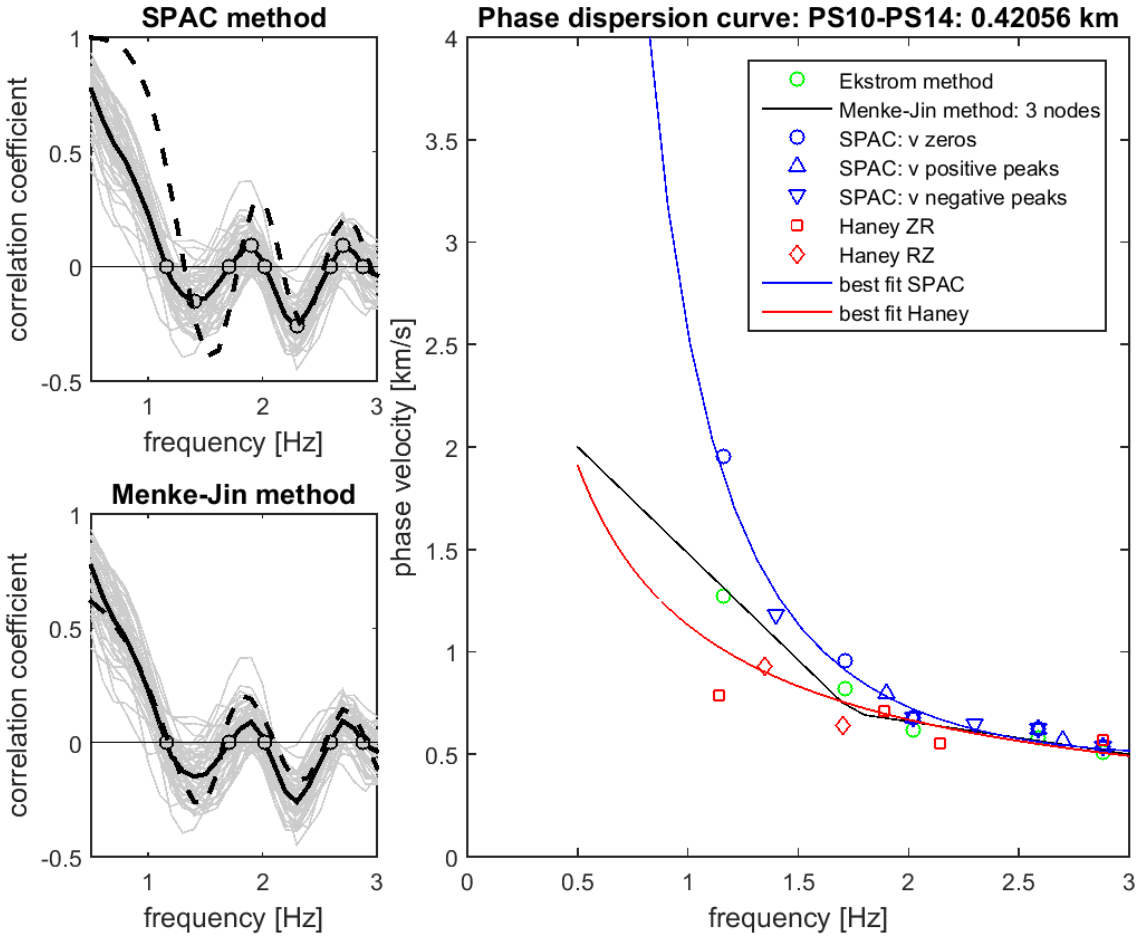

Figure 3.13: Example of phase dispersion curves between stations *PS10* and *PS14*, 420.5 m apart, obtained using the different methods described above. The green open circles are the phase velocities estimated using the zero-crossings of the vertical-vertical (ZZ) cross-correlation [34]; the black solid line is the curve obtained from the grid search of 3 nodes suggested by Menke and Jin [58]. The blue solid line and blue markers are related to the SPAC method. The red markers (included the green open circles) and the red solid line are linked to the Haney et al. [41] method, as described above.

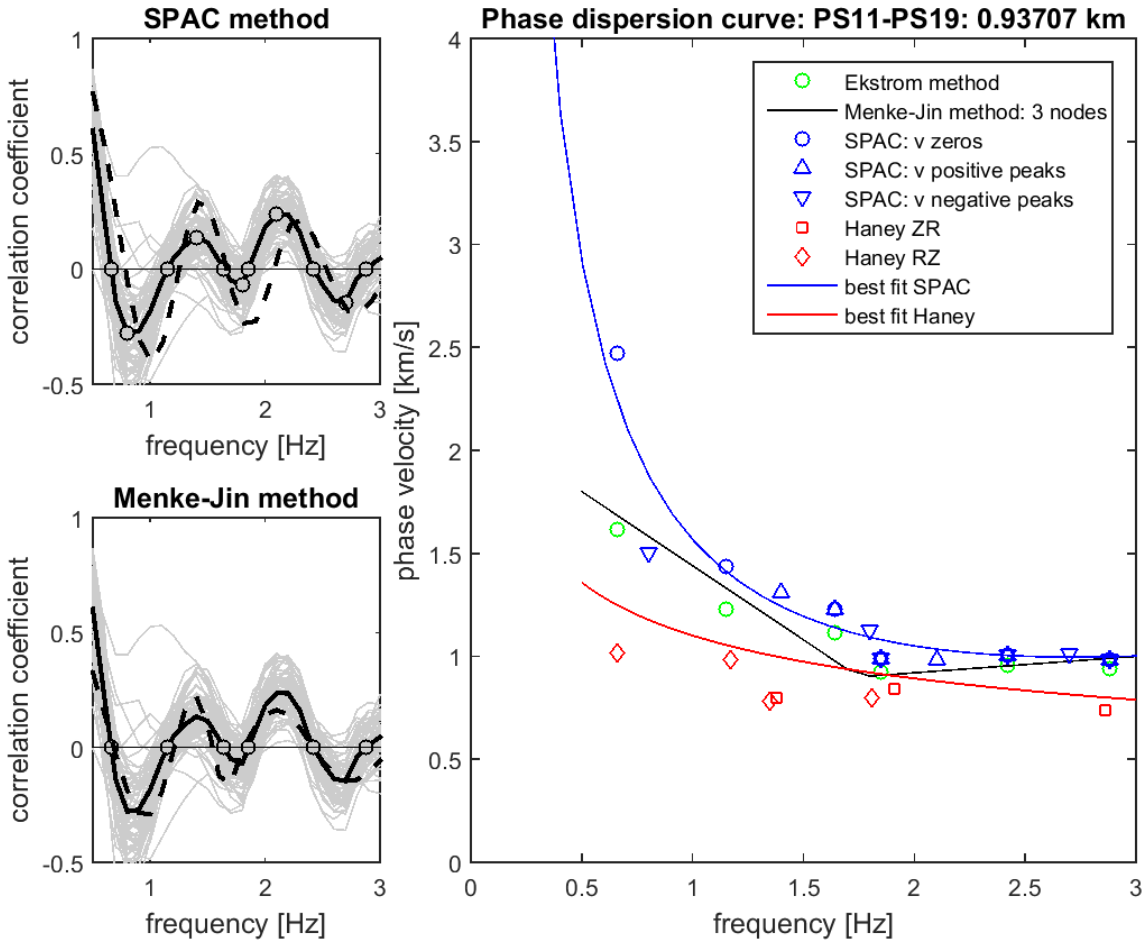

Figure 3.14: Similar plot as Fig. 3.13 between stations *PS11* and *PS19*, 937 m apart.

As we can see, different methods give comparable results suggesting that phase dispersion curves are reasonable and consistent if we assume the original idea of Aki [1] is valid. Not only are the dispersion curves in the same range, but we have also observed that these curves give a calculated average autocorrelation function similar to the observed one. We could not verify the validity of the dispersion curves obtained with the Haney et al. [41] method for the missed zero-crossings issue, but the similarity of it with the other tested estimated curves provide us that even this method and its relative dispersion curve might be considered usable.

All these techniques seem to confirm the observations described above, that it is

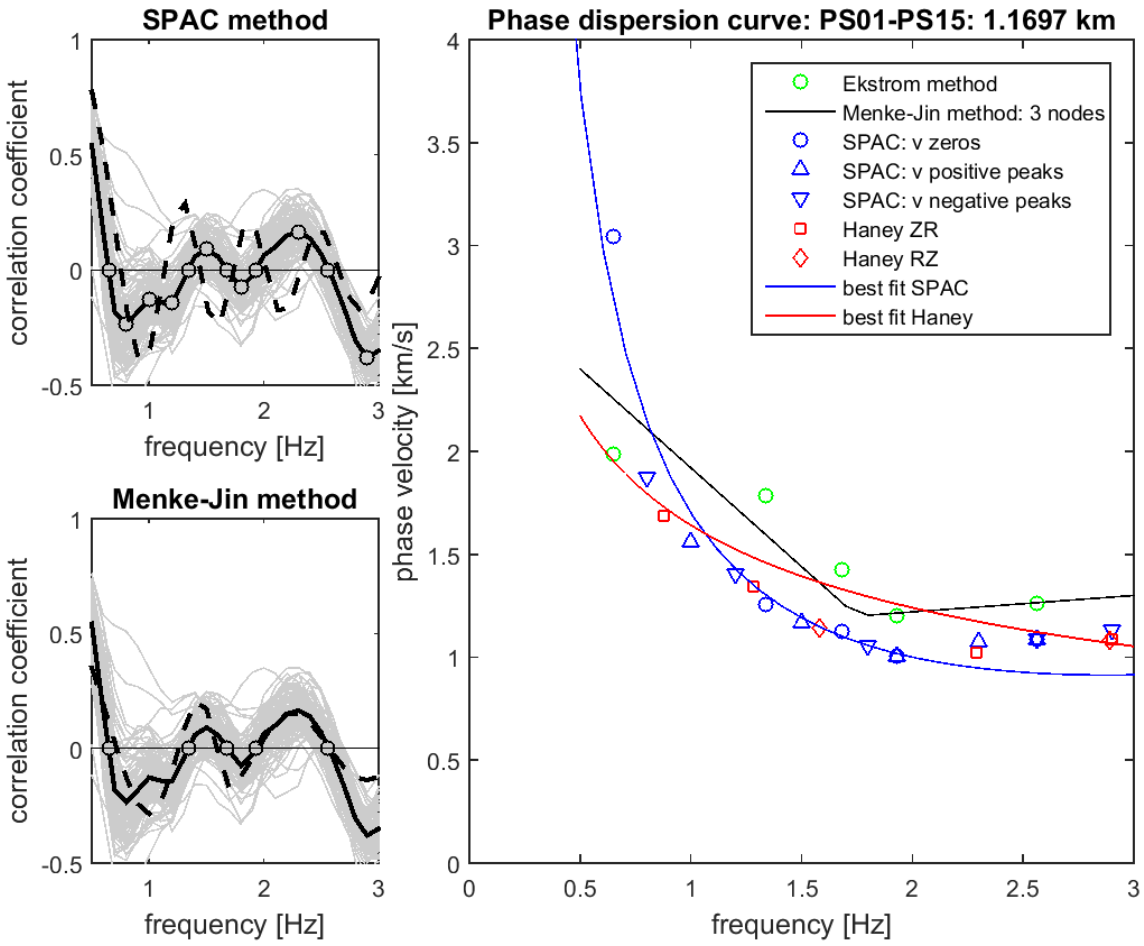

Figure 3.15: Similar plot as Fig. 3.13 between stations *PS01* and *PS15*, 1.17 km apart.

possible to have relatively high phase velocities in a active volcanic system and the relatively constant phase velocities above 1-1.5 Hz. Moreover above this threshold all dispersion curves seem to have very similar velocitites, whereas below it the solution is not unique; in particular the SPAC method proposed by Chouet et al. [20] and Saccorotti et al. [73] differs a lot respect to the other approaches showing very high velocities.

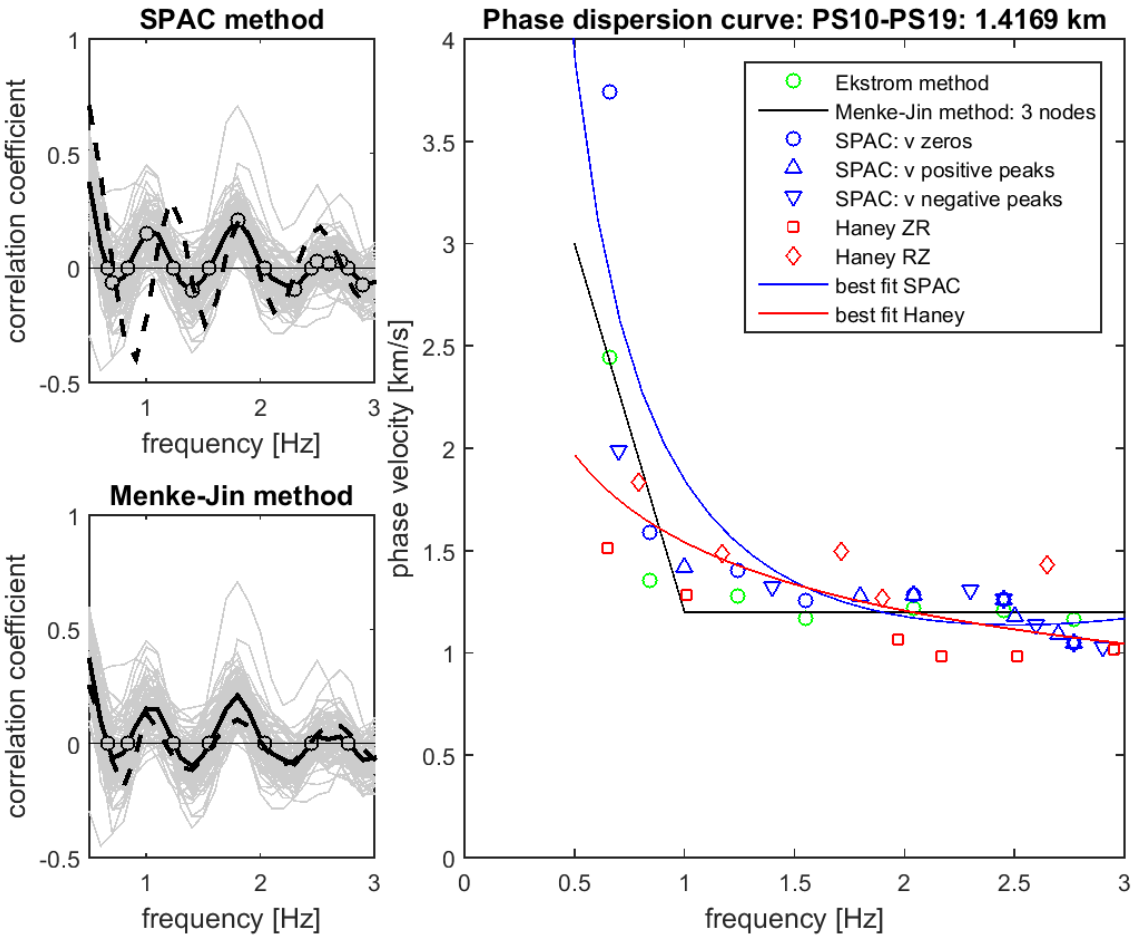

Figure 3.16: Similar plot as Fig. 3.13 between stations *PS10* and *PS19*, 1.42 km apart.

3.2.5 SPAC-Ekström technique

We noted that, except for the first phase velocity calculated using zero crossings in the SPAC, the dispersion curves found with the Ekström method and that obtained by the SPAC method showed the same trend. In particular, the phase velocities found using the zero-crossings, maxima and minima approaches were nearly the same as those found focusing only on the zero-crossings in the Ekström equation (eq. 2.3), especially at higher frequencies. In fact we were able to fit the same trend for the majority of our station pairs. The apparent consistency in the results allowed us to try

to fit these points with a power-law; we used the same process illustrated by Chouet et al. [20] and Saccorotti et al. [73], that is a grid search to find the parameters A, b and c in the both eq. 2.2 (Fig. 3.17). Even though the Bessel functions described by these two formulas do not fit the average autocorrelation function as well as that of the Menke and Jin [58] grid search, the result could not be discarded at all; in fact the dispersion curve is smoother than the Menke-Jin one and also the Bessel function might be acceptable.

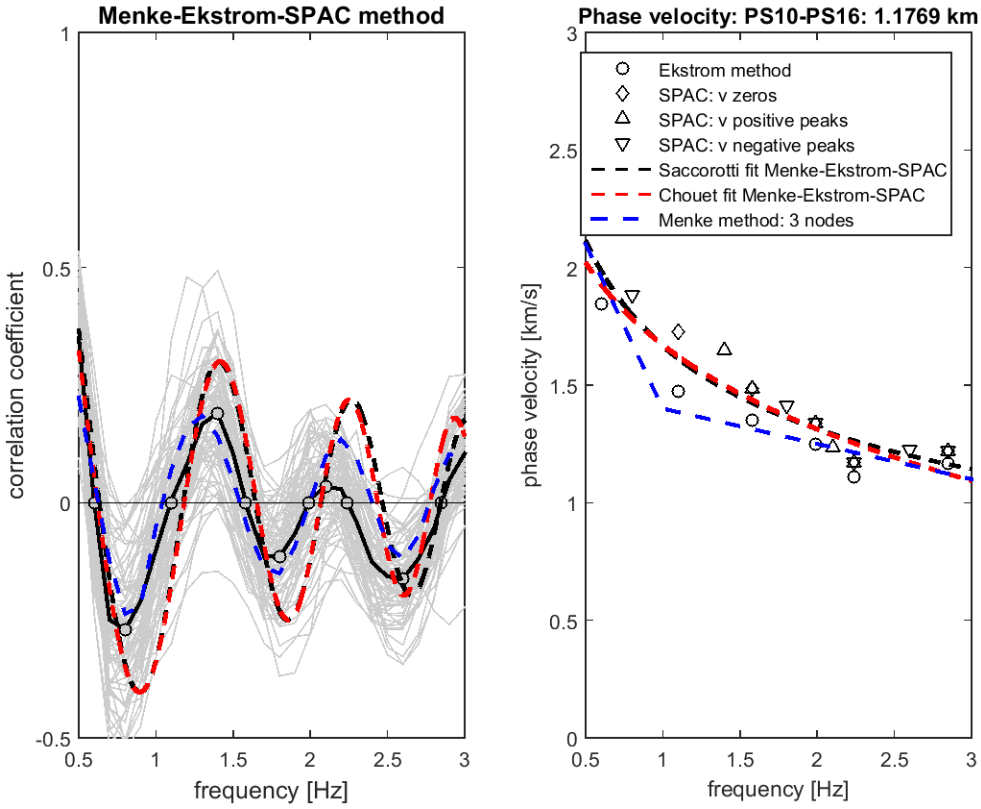

Figure 3.17: Example of phase dispersion curve between stations *PS10* and *PS16*, 1.18 km apart, obtained fitting the results of zero-crossings of the Ekström et al. [34] method and the zero-crossings, maxima and minima of Chouet et al. [20] and Saccorotti et al. [73]. The red and black dashed lines represent the fitting using both eq. 2.2, while the blue dashed line is the comparison with the Menke-Ekström approach.

However, this new approach is based on the discarding of the first phase velocity calculated using the first zero-crossing in the SPAC method, because its value appeared too high in almost all cross-correlations. Note that both formulas of eq. 2.2 give almost the same result (Fig. 3.17, look the red and black dashed lines).

Chapter 4

Discussion

The initial goal of this work was focused on creating a 3D tomographic model of Pacaya volcano using the ambient noise surface wave analysis. The commonly-employed approach described in detail by Bensen et al. [6] and applied widely including at active volcanic systems such as Montserrat volcano [9] and Okmok volcano [56] is powerful, but it requires at least one month of data and inter-station distances greater than two-three wavelengths. Given the close station spacing at Pacaya, this method would not work for frequencies below 0.5 Hz that typically dominate the ambient noise record at broadband stations.

We applied this technique to relatively high frequencies, knowing that we had only 4-7 days of cross-correlations and distances between stations were often smaller than 2 wavelengths for the lowest frequencies. The group dispersion curves were affected by the low SNR and we limited a further analysis to shallow 1D shallow velocity models of:

- the entire volcano (*"All Pacaya"*);
- the old ancestral edifice (*"Old Pacaya"*);
- new MacKenney cone (*"New Pacaya"*).

Although were not able to identify differences between these models, our models were

comparable to that found by Lanza et al. [46] with a small aperture array analysis of data from 2011.

Trusting all single group dispersion curves was impossible for the presence of many spikes more probably due to the low SNR. This error becomes "attenuated" when the number of days of data is large enough to increase the SNR allowing to find reliable dispersion curves. The problem of limited data can be overcome by using the approach of the SPAC (SPatial AutoCorrelation) in which only cross-correlations of selected time windows of many minutes are chosen. Windows are chosen such that there are no events; the resulting correlation functions are then stacked. By selecting hundreds of time intervals, which is easy to find even if there are just a few available days, we were able to increase the SNR and have reliable results without modifying the original data as we did using the temporal normalization and the spectral whitening with the Bensen et al. [6] method.

The SPAC method, based on the original idea of Aki [1], is usually used in a volcano with a small aperture array (from 100 to 500-600 meters) having stations located at same distances. Reliable phase dispersion curves and the successive shallow velocity structure beneath the array are found in many active volcanic system such as Stromboli volcano [20], Puu Oo crater in Hawaii [35], Kilauea volcano [73], Arenal volcano in Costa Rica [61], Pacaya volcano [46].

However, this technique described in detail by Chouet et al. and Saccorotti et al. in their papers was not ever applied on a pair of stations with distances greater than 600 meters. Assuming the idea of stochastic random wave-field is valid [1], we used 139 selected time windows of 24-360 seconds long to make cross-correlations in the time-domain, similarly to the process used for the SPAC. The resulting autocorrelation functions describe a reliable pattern, even though some intervals were below 1 minute long. Moreover, the observed correlation coefficients seem to follow a Bessel function trend up to 3 Hz, as expected by Aki sixty years ago. This suggests that this approach is reliable even considering only a pair of stations up to about 1.5 km apart.

The similarity of the results between the vertical-vertical (ZZ) cross-correlations and the Bessel function allowed us to apply the same process to find phase dispersion curves as described in Chouet et al. [20] and Saccorotti et al. [73], considering the zero-crossings, maxima and minima. Phase velocities at these points are calculated using eq. 3.1 assuming the autocorrelation function as a wave and we have obtained results that follow an expected trend similar to a surface wave dispersion curve. These velocities are comparable to those calculated with other different methods such as the Ekström et al. [34] and the Haney et al. [41] procedures. These approaches are usually applied to estimate phase dispersion curves from cross-correlations in the frequency-domain, but appear to work well when cross-correlations are computed using the time-domain, SPAC-type short windows approach described above.

The Haney et al. method [41], in particular, is an evolution of the Ekström technique considering the zero-crossings not only of the vertical-vertical (ZZ) cross-correlation but also the vertical-radial one (ZR). We found that these two tools can be also applied to find consistent phase dispersion curves comparable with the other methods described above. The only requirement is that the autocorrelation functions look like a Bessel function. If this is not respected, it is possible to correct the missed zero-crossings, but this becomes not more completely objective. The correction by the missed or extra zero-crossings affects more the Haney et al. [41] method rather than the Ekström et al. [34] procedure, simply because it needs three correlation coefficients curves, that is the vertical-vertical (ZZ as Ekström one), vertical-radial (ZR) and the radial-vertical (RZ) cross-correlations. To avoid the correction of the missed zero-crossings we improved the SPAC method considering the phase velocities estimated on zero-crossings of the Ekström approach and zero-crossings, maxima and minima of the SPAC. Fitting all these points using a power-law equation in the forms of eq. 2.2 we found that the resulting phase dispersion curve describes a Bessel function similar to the autocorrelation function. This new observation and procedure does not require the correction for the missed zero-crossings and provides reliable and

consistent surface wave dispersion curves.

In Fig. 3.17 we compared our result with that obtained using the first step of the Menke and Jin [58] method. Even though the latter one fits the autocorrelation function better, because it also accounts for the amplitude correction, the relative dispersion curve is not smooth.

All of these applied methods require the similarity of the autocorrelation function to a Bessel function in order to be able to apply the original idea of Aki [1] and his formula (eq. 2.1) which connects the correlation coefficient to the phase dispersion curve through a Bessel function. This condition occurs in Pacaya volcano only considering a pair of stations from 300 m up to 1.5 km apart. In fact, for small distances (we did not have stations closer than 300 meters) the techniques that use only the zero-crossings give few phase velocities. For distances greater than 1.5 km, instead, the waveforms recorded by the two stations are not well correlated at these low frequencies, at least up to 3 Hz.

Figures 3.13, 3.14, 3.15 and 3.16 show that different methods to find the surface wave dispersion curves yield similar results for different inter-station distances, suggesting that the velocities we found are reasonable. However, these phase dispersion curves indicate velocities higher than those expected in an active volcanic system and, in particular the behavior of these curves becomes pretty flat above 1-1.5 Hz. The combination of these two features might indicate that higher-order modes, or body waves may contribute to the correlation functions. The contribution of body waves seems likely due to many scatterers in the volcanic edifice. We can expect that topography and small-scale variations in velocity might produce scattered waves as a result of refraction, reflection and conversion of P and S waves.

The most remarkable difference between surface waves and body waves involves the fact that the former are dispersive; that is, velocity is related to the frequency of the wave. Body waves are not dispersive. Therefore, looking at the dispersion curves, we expect that the velocity of surface waves decreases as a function of frequency, while

that of body waves should be a flat line whose value represents an average velocity of the propagating medium. Moreover, this averaged velocity should be dependent of the distance between the stations, because we can think that greater is the distance separating a pair of stations deeper is the depth that body waves can reach; the resulting velocities should be higher. In other words, if in our dispersion curves we see a relationship between phase velocity and distance between stations we may be facing a contribute of body waves together with dispersive surface waves, or more likely a mixture of them forming scattered waves. The reason of the presence of scattered waves might be due to the seismic station configuration in proximity of the Pacaya vent; in fact, being most of the wave paths around the volcanic conduit, the presence of heterogeneities can lead these waves to be trapped and scattered many times.

We tried to confirm our hypothesis by plotting the values of phase velocity for different frequencies (*0.5*, *1.0*, *1.5*, *2.0*, *2.5*, *3.0 Hz*) as a function of distance between two stations using the Menke and Jin [58] and the Haney et al. [41] methods (see Appendix E and F). Fig. 4.1 and Fig. 4.2 show the results using these two different techniques. It is clear that using the Haney approach this relationship between phase velocity as a function of inter-station distance becomes consistent, in particular for all chosen frequencies. This is less evident applying the Menke-Jin process, but it is possible noting that above 1.5 - 2.0 Hz the linear trend also appears. This dependence becomes very clear around 2.0 Hz. A further difference between body and surface waves is the different particle motion, but it was difficult to analyze.

Considering this phase velocity - inter-station distance dependence, we tried to use the results of the 26 dispersion curves obtained using the Menke-Jin [58] and Ekström et al. [34] comparison and the 66 surface wave dispersion curves estimated with the Haney et al. [41] approach, to analyze velocity variations at Pacaya volcano at different frequencies. This stage is the step preceding the inversion of the surface wave dispersion curves to create a 2D and 3D seismic tomography. This first result,

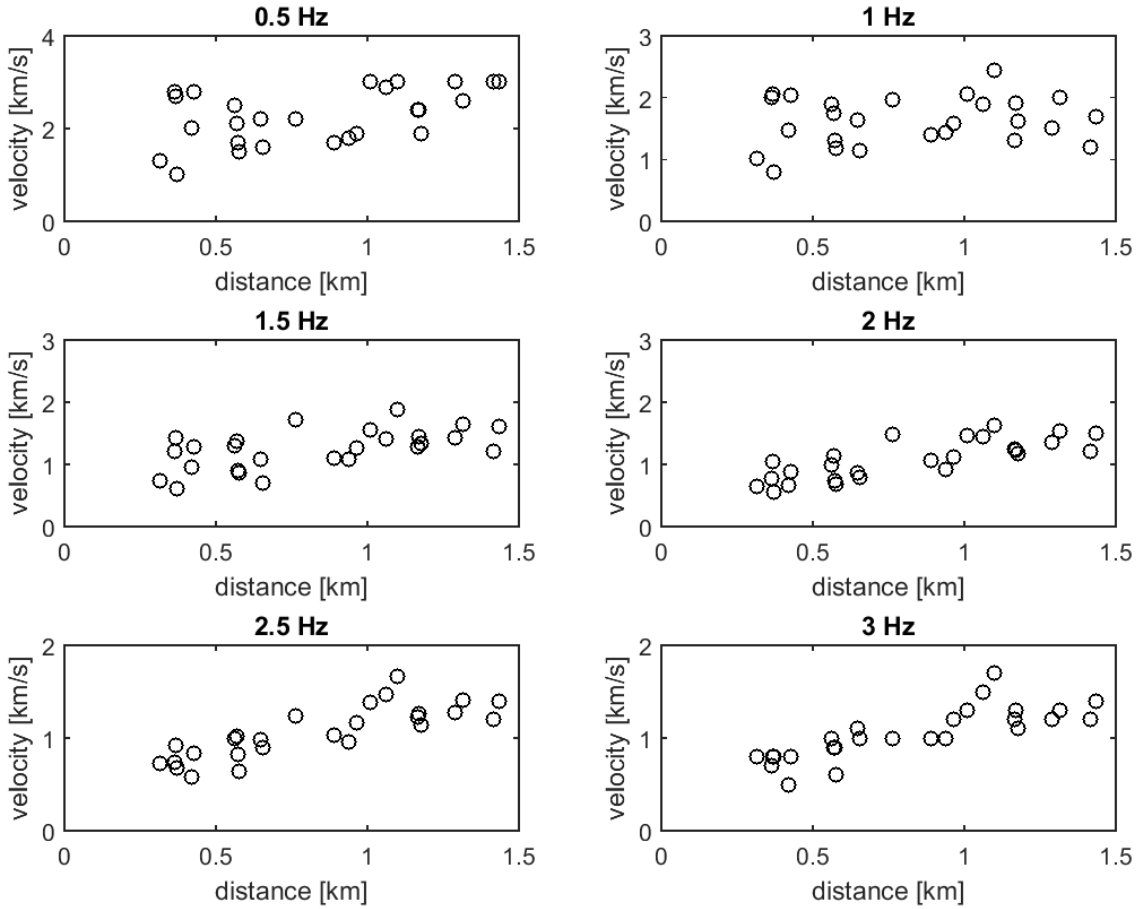

Figure 4.1: Rayleigh phase velocity as a function of distance between a pair of stations using the Menke and Jin [58] approach. We used 26 dispersion curves in which the Menke-Jin and the Ekström methods overlap. Each panel represents this relation for a specific frequency; we chose 0.5, 1.0, 1.5, 2.0, 2.5 and 3.0 Hz. Note that above 1.5-2.0 Hz a linear relationship between velocities and distances appears.

showed in Fig. 4.4 and Fig. 4.5, allows to recognize the main characteristic features in the Pacaya volcanic system. In fact, even before doing the inversion, horizontally and vertical velocity anomalies should show up. Even though each subfigure is referred in 2 dimensional space, the combination of all 6 panels allows to build a sort of 3D geometry of the entire volcano. The key concept involves the known idea that surface waves are dispersive, so waves characterized by lower frequency travel deeper than those with higher frequencies. The application of this theoretical idea is also shown

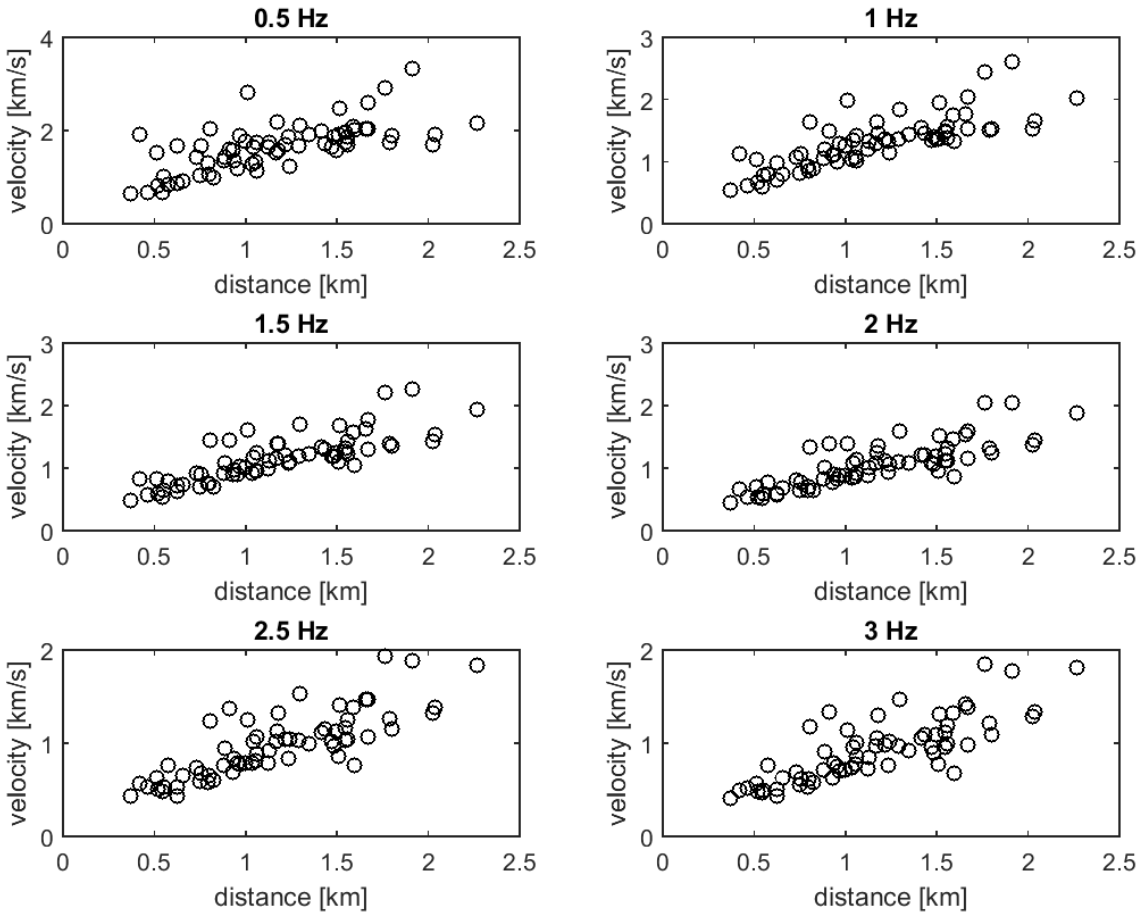

Figure 4.2: Rayleigh phase velocity as a function of distance between a pair of stations using the Haney et al. [41] approach and the Saccorotti et al. [73] formula (eq. 2.2) to fit the data. We used 66 dispersion curves in which it was possible correcting the missed zero-crossings in all three cross-correlations (ZZ, ZR and RZ). Each panel represents this relation for a specific frequency; we chose 0.5, 1.0, 1.5, 2.0, 2.5 and 3.0 Hz. A linear relationship between velocities and distances is evident for all selected frequencies.

in the inversion of the dispersion curve found using the Bensen et al. [6] approach (Fig. 3.8). The interpretation of these two results is hard, in particular because of dependence of velocity - inter-station distance, so short distances between two stations should show smaller surface wave phase velocities than a pair of stations farther. Each subfigure of Fig. 4.4 and 4.5 represents the phase velocity of the surface wave at a particular frequency (*0.5*, *1.0*, *1.5*, *2.0*, *2.5* and *3.0 Hz*). This means that the 2D

panel at *0.5 Hz* is located at the bottom of the 3D cubic (deeper) and the *3.0 Hz* layer at the top (shallower depth) (Fig. 4.3).

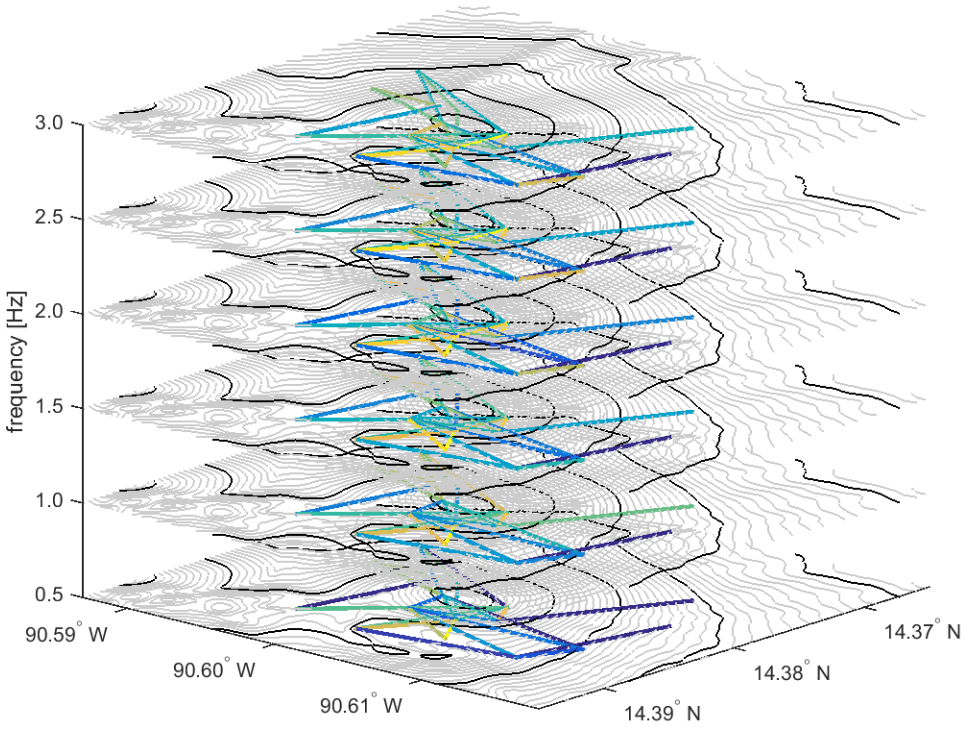

Figure 4.3: 3D cubic of the 6 panels represented in Fig. 4.4. Lower frequencies mean greater depth.

Assuming this relationship not too relevant and influential in the final result, in Fig. 4.4 we cannot see a very distinct pattern, but we can recognize some interesting features such as relative low velocities between stations *PS08* and *PS14* and stations *PS09* and *PS10*, both located in the northwestern side of the MacKenney vent. This is particular evident focusing on *0.5 Hz* (highest depth). It doesn't seem related to the velocity - inter-station distance dependence because other pairs of stations with the same distance have higher velocities. However the low velocity in the northwestern side of the volcano crater appears clear at all frequencies suggesting the possibility of

a high-temperature or fractured zone below. The second hypothesis, a very fractured zone, seems to be likely due to the collocation with the 2010 collapse trough. At shallower depth a remarkable feature is represented by a low velocity zone near the pair *PS11 - PS18* at almost all frequencies. This area coincides with the position of the vents of older flows (*OL-3* in the paper of Schaefer et al. [74]). Moreover, at *1 Hz* also the southeastern side of the MacKenney vent seems to be characterized by a relative low velocity describing a NW-SE trending. Even though we are looking at only 26 phase dispersion curves obtained using the comparison between the Menke and Jin [58] and the Ekström et al. [34] methods, it might be evidence of a NNW-SSE volcanic rift zone (VRZ) of Pacaya volcano, already suggested by Schaefer et al. [74]. This preferential direction should be dominated by low velocities and relative high temperature, being the privileged area for the magma ascent. Basing on the poor result of these 26 phase dispersion curves we are not be able to confirm or reject the hypotesis of the presence of a shallow magma body [7, 29, 30, 31, 32, 38, 60, 68, 74, 75, 84, 89], but, assuming a shallow magma chamber, it would be at a depth less than the depth outlined by *0.5 Hz*, because at higher frequencies the relative velocities between pairs of stations decrease suggesting higher temperature zones respect deeper areas.

Considering more reliable the results through the comparison between the Menke and Jin [58] and the Ekström et al. [34] methods, in Fig. 4.5 are represented the results of the 66 phase dispersion curves estimated using the Haney et al. [41] approach. We have seen that this technique, including the correction for the missed zero-crossings of the vertical-vertical (ZZ), vertical-radial (ZR) and radial-vertical (RZ), cannot be considered completely reliable for Pacaya volcano due to the small number of available days (4-7). Moreover, it seems to be more influenced by the velocity - inter-station distance relationship than the comparison between the Menke-Jin and the Ekström methods (Fig. 4.2). In fact all six panels show almost the same colors representing the similar features at all depths (relative velocities). Nevertheless, we can recognize some differences at different depths: in particular it appears

clear that velocities between stations *PS04* - *PS06* and *PS16* - *PS18* are relatively low at *0.5 Hz*, whereas these increase at shallower depths. With the opposite trend it seems to be the behavior of the central area around the vent where remarkable changes involve stations *PS10* - *PS14* and *PS01* - *PS12*. However, in this case it is not possible recognizing an evident NW-SE low-velocity trend interpreted as the VRZ.

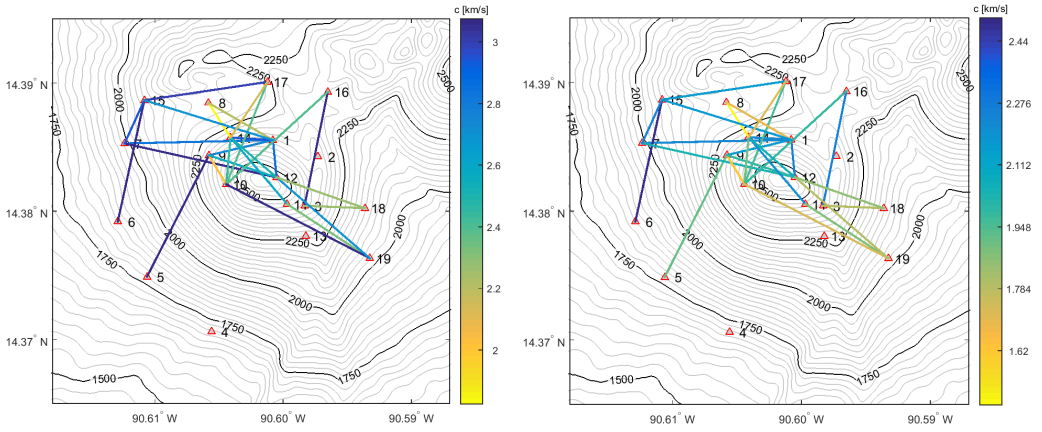

(a) 0.5 Hz (b) 1.0 Hz

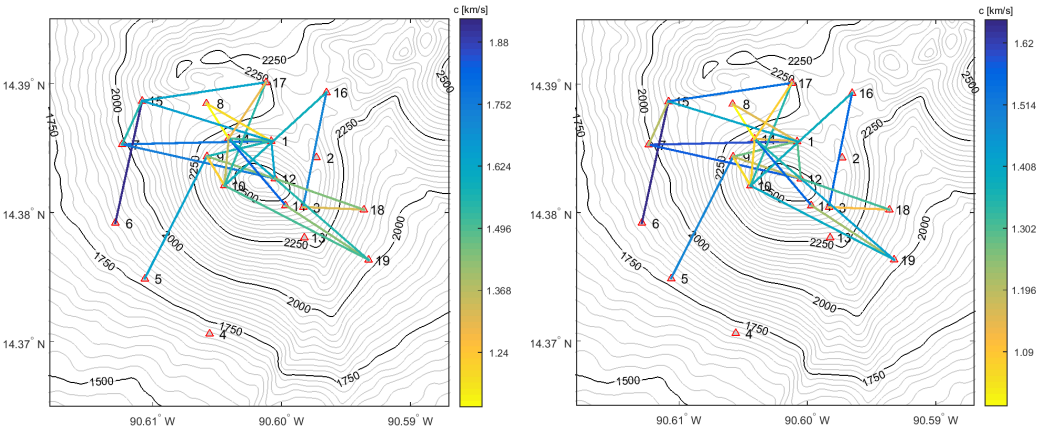

(c) 1.5 Hz (d) 2.0 Hz

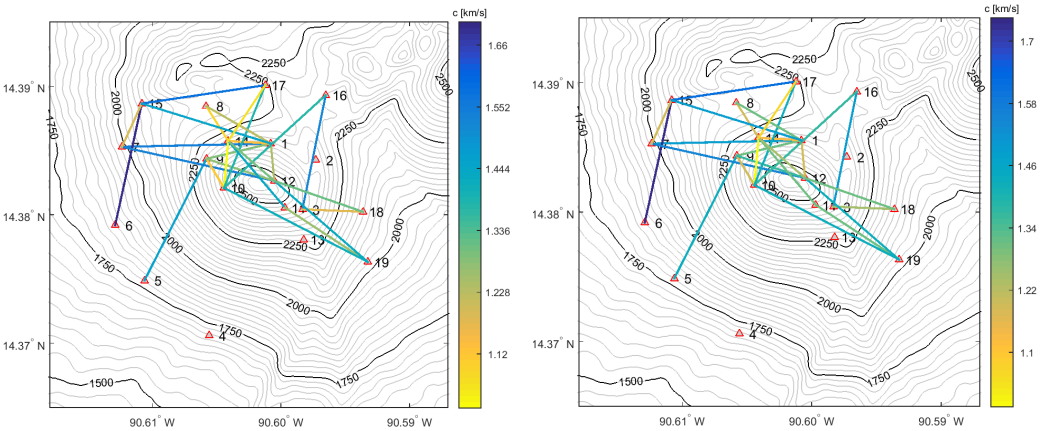

(e) 2.5 Hz (f) 3.0 Hz

Figure 4.4: 26 phase velocities at 6 different frequencies (0.5, 1, 1.5, 2, 2.5 and 3 Hz) estimated using the surface wave dispersion curves of the comparison between the Menke and Jin [58] and the Ekström et al. [34] methods.

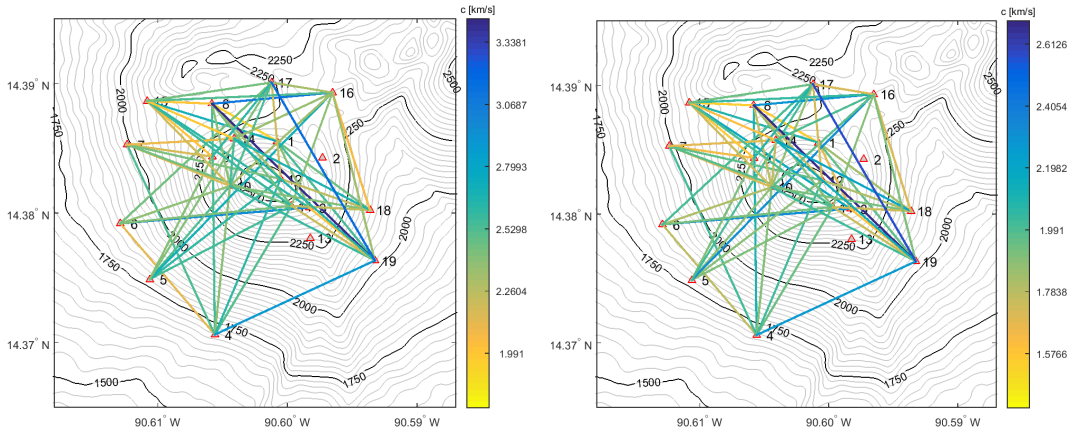

(a) 0.5 Hz

(b) 1.0 Hz

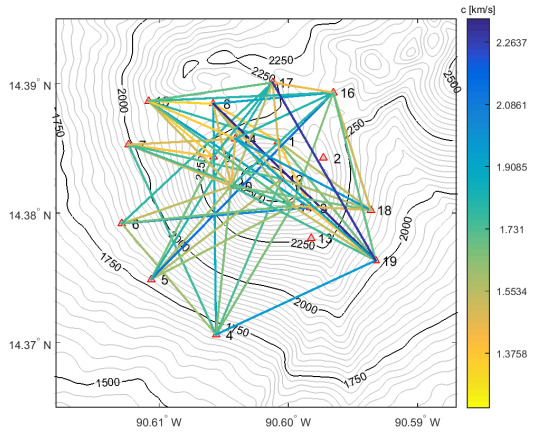

(c) 1.5 Hz

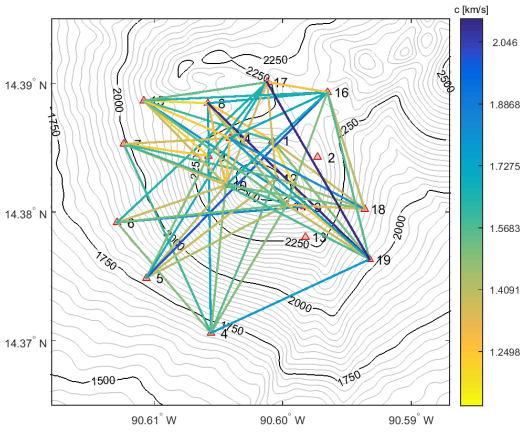

(d) 2.0 Hz

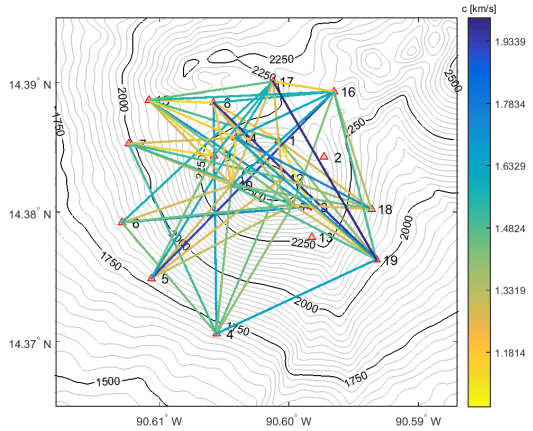

(e) 2.5 Hz

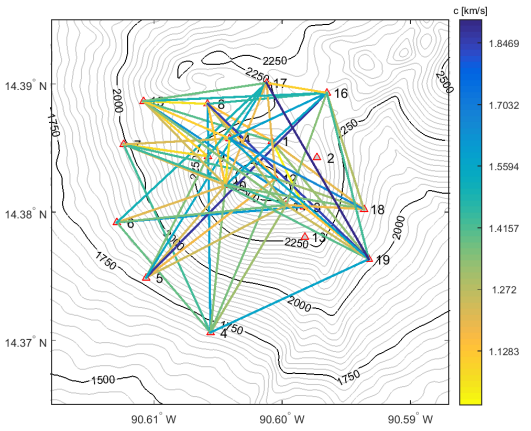

(f) 3.0 Hz

Figure 4.5: 66 phase velocities at 6 different frequencies (0.5, 1, 1.5, 2, 2.5 and 3 Hz) estimated using the surface wave dispersion curves of the Haney et al. [41] method.

Chapter 5

Conclusion

The essential things that need to create a 3D ambient noise tomography are the surface wave dispersion curves. There are several methods to determine them, but all of them require a large number of available days of data and inter-station distances greater than 2-3 wavelengths to give a reliable SNR. For temporary arrays in active volcanic regions, it is more common to have few days of data and distances between stations smaller than 2 wavelengths. This might be a problem, but we showed that the SPAC (SPatial AutoCorrelation) approach, usually applied to find the shallow velocity structure beneath a small aperture array, gives reliable surface wave dispersion curves even used for only a pair of distant stations.

We suggest to use cross-correlations of hundreds time windows to avoid low SNR and errors of normalization and spectral whitening whether the available days of data are small. We noted that this SPAC-type short windows correlations can be applied also for the Ekström and Haney techniques, commonly made in the frequency-domain. Comparison with different techniques, all based on the idea of Aki (1957) of stochastic wave-field, indicate that these methods give consistent phase dispersion curves. In particular, we found relatively high Rayleigh phase velocities and these curves become flat above *1.5 - 2 Hz* suggesting the possible presence of body waves within the surface waves. This hypothesis might be confirmed with the linear relationship between phase velocities and inter-station distances found for many frequencies.

Plotting phase velocities for pairs of stations at different frequencies using the dispersion curves obtained using the comparison between the Menke-Jin and the Ekström et al. methods, a probable low-velocity area oriented about NW-SE seems to show up, interpreted as the volcanic rift zone (VRZ).

Finally, future detailed studies and longer surveys are suggested to create a complete 3D ambient noise tomography of this active volcano, analyzing in particular the relation between the volcanic behavior and the local tectonics.

References

[1] Aki, K. Space and time spectra of stationary stochastic waves, with special reference to microtremors. *Bulletin of the Earthquake Research Institute 25* (1957), 342–351.

[2] Aki, K. Correlational study of near earthquake waves. *Bulletin of the Earthquake Research Institute 37* (1959), 207–232.

[3] Aki, K. A note on the use of microseisms in determing the shallow structures of the Earth's crust. *Geophysics 30* (1965), 665–666.

[4] Andres, R. L., and Kasgnoc, S. D. A time-averaged inventory of subaerial volcanic sulfur emissions. *Journal of Geophysical Research 103* (1998), 25251–25261.

[5] Bardintzeff, J. M., and Deniel, C. Magmatic evolution of Pacaya and Cerro Chiquito volcanological complex. Guatemala. *Bulletin of Volcanology 54*, 4 (1992), 267–283.

[6] Bensen, G. P., Ritzwoller, M. H., Barmin, M. P., Levshin, A. L., Lin, F., Moschetti, M. P., Shapiro, N. M., and Yang, Y. Processing seismic ambient noise data to obtain reliable broad-band surface wave dispersion measurements. *Geophys. J. Int. 169* (2007), 1239–1260.

[7] Bohnenberg, O. Report on active volcanoes in Central America during 1957 to 1965. Unpublished report to the International Volcanological Association, 1966.

[8] Brenguier, F., Shapiro, N. M., Campillo, M., Ferrazzini, V., Duputel, Z., Coutant, O., and Nercessian, A. Toward forecasting volcanic eruptions using seismic noise. *Nature 1* (2008), 126–130.

[9] Brenguier, F., Shapiro, N. M., Campillo, M., Nercessian, A., and Ferrazzini, V. 3-D surface wave tomography of the Piton de la Fournaise volcano using seismic noise correlations. *Geophysical Research Letters 34* (2007), 5.

[10] Burkart, B., and Self, S. Extension and rotation of crustal blocks in northern Central America and effect on the volcanic arc. *Geology 13* (1985), 22–26.

[11] Cameron, B. I., Walker, J., Carr, M. J., Patino, L. C., Gómez, R. O. M., and Feigenson, M. D. Flux versus decompression melting at stratovolcanoes in southeastern Guatemala. *Journal of Volcanology and Geothermal Research 119* (2002), 21–50.

[12] Campillo, M. Phase and correlation in random seismic fields and the reconstruction of the Green function. *Pure Appl. Geophys. 163* (2006), 475–502.

[13] Campillo, M., and Paul, A. Long-range correlations in the diffuse seismic coda. *Science 299* (2003), 547–549.

[14] Carr, M. J. Symmetrical and segmented variation of physical and geochemical characteristics of the Central American Volcanic Front. *Journal of Volcanology and Geothermal Research 20* (1984), 231–252.

[15] Carr, M. J., Feigenson, M. D., Patino, L. C., and Walker, J. A. Volcanism and geochemistry in Central America: progress and problems. In *Inside the Subduction Factory*, J. Eiler, Ed., vol. 138. Washington DC, 2003, pp. 153–179.

[16] Carr, M. J., and Stoiber, R. E. Volcanism. In *The Caribbean Region. The geology of North America*, G. Dengo and J. E. Case, Eds., vol. H. 1990, pp. 375–391.

[17] Chávez-García, F. J., Rodríguez, M., and Stephenson, W. R. An alternative approach to the SPAC analysis of microtremors: exploiting stationary of noise. *Bulletin of the Seismological Society of America 95*, 1 (2005), 277–293.

[18] Cho, K. H., Herrmann, R. B., Ammon, C. J., and Lee, K. Imaging the upper crust of the Korean Peninsula by surface-wave tomography. *Bull. Seism. Soc. Am. 97*, 1B (2007), 198–207.

[19] Chouet, B. New methods and future trends in seismological volcano monitoring. In *Monitoring and Mitigation of Volcano Hazards*, R. Scarpa and R. I. Tilling, Eds. Springer, New York, NY, 1996, pp. 23–97.

[20] Chouet, B., Luca, G. D., Milana, G., Dawson, P., Martini, M., and Scarpa, R. Shallow velocity structure of Stromboli volcano, Italy, derived from small-aperture array measurements of Strombolian tremor. *Bulletin of the Seismological Society of America 88* (1998), 653–666.

[21] Conway, F. M. *Construction patterns and timing of volcanism at the Cerro Quemado, Santa Maria, and Pacaya volcanoes, Guatemala.* PhD thesis, Michigan Technological University, Houghton, Michigan, 1995.

[22] Conway, F. M., Diehl, J. F., and Gómez, R. O. M. Paleomagmatic constraints on eruption pattern at Pacaya composite volcano, Guatemala. *Bulletin of Volcanology 55* (1992), 25–32.

[23] Dalton, M. P., Waite, G. P., Watson, I. M., and Nadeau, P. A. Multiparameter quantification of gas release during weak Strombolian eruptions at Pacaya Volcano, Guatemala. *Geophysical Research Letters 37* (2010), 5.

[24] Decker, R. W. State-of-the-art in volcano forecasting. *Bulletin of Volcanology 33* (1974), 372–393.

[25] Demets, C., Gordon, R. G., Argus, D. F., and Stein, S. Current plate motions. *Geophys. J. Int. 101* (1990), 425–478.

[26] Derode, A., Larose, E., Tanter, M., de Rosny, J., Tourim, A., Campillo, M., and Fink, M. Recovering the Green's function from field-field correlations in a open scattering medium. *J. acoust. Soc. Am. 113* (2003), 2973–2976.

[27] Dziewonski, A. M., Bloch, S., and Landisman, M. A technique for the analysis of transient seismic signals. *Bull. Seism. Soc. Am. 59* (1969), 427–444.

[28] Eggers, A., Krausee, J., Rush, H., and Ward, J. Gravity changes accompanying volcanic activity at Pacaya volcano, Guatemala. *Journal of Volcanology and Geothermal Reseach 1* (1976), 229–236.

[29] Eggers, A. A. *The geology and petrology of the Amatitlán quadrangle. Guatemala.* PhD thesis, Darmounth College, Hanover, New Hampshire, 1971.

[30] Eggers, A. A. Geological map of the Amatitlán Quadrangle, Guatemala. Tech. rep., 1975. scale 1:50,000.

[31] Eggers, A. A. Temporal gravity and elevation changes at Pacaya volcano, Guatemala. *Journal of Volcanology and Geothermal Research 19* (1983), 223–237.

[32] Eichelberger, J. C., and McGetchin, T. R. Petrogenesis of the 1973 Pacaya Lavas, Guatemala. Int. Symp. on Volcanology, IAVCEE, pp. 1–13.

[33] Ekström, G. Love and Rayleigh phase-velocity maps, 5-40 s, of the western and central USA from USArray data. *Earth Planet. Sci. Lett. 402* (2013), 42–49.

[34] Ekström, G., Abers, G. A., and Webb, S. C. Determination of surface-wave phase velocities across USArray from noise and Aki's spectral formulation. *Geophysical Research Letters 36* (2009), 5.

[35] Ferrazzini, V., Aki, K., and Chouet, B. Characteristics of seismic waves composing Hawaiian volcanic tremor and gas piston events observed by near-source array. *Journal of Geophysiscal Research 96* (1991), 6199–6209.

[36] Franco, A., Lasserre, C., Lyon-caen, H., Kostoglodov, V., Molina, E., Guzman-Speziale, M., Monterroso, D., Robles, V., Figueroa, C., Amaya, W., Barrier, E., Chiquin, L., Moran, S., Flores, O., Romero, J., Santiago, J. A., Manea, M., and Manea, V. C. Fault kinematics in northern Central America and coupling along the subduction interface of the Cocos Plate, from GPS data in Chiapas (Mexico), Guatemala and El Salvador: kinematics in northern Central America. *Geophys. J. Int. 189* (2012), 1223–1236.

[37] Gill, J. B. *Orogenic andesites and plate tectonics*. Springer, New York, 1981.

[38] Gómez, R. O. M. Volcanological map of the 1961-2010 eruption of Volcän de Pacaya, Guatemala. Master's thesis, Michigan Technological University, Houghton, Michigan, 2009.

[39] Gómez, R. O. M., Rose, W. I., Palma, J. L., and Escobar-Wolf, R. Notes on a map of the 1961-2010 eruptions of Volcán de Pacaya, Guatemala. *Geological Society of America Digital Map Chart Series 10* (2012), 10.

[40] Guzman-Speziale, M. Active seismic deformation in the grabens of northern Central America and its relationship to the relative motion of the North America-Caribbean plate boundary. *Tectonophysics 337* (2001), 39–51.

[41] Haney, M. M., Mikesell, T. D., van Wijk, K., and Nakahara, H. Extension of the spatial autocorrelation (SPAC) method to mixed-component correlations of surface waves. *Geophys. J. Int. 191* (2012), 189–206.

[42] Herrin, E. E., and Goforth, T. T. Phase-matched filters: Application to the study of Rayleigh waves. *Bull. Siesm. Soc. Am. 67* (1977), 1259–1275.

[43] Herrmann, R. B. Computer programs in seismology: an evolving tool for instruction and research. *Seismological Research Letters 84* (2013), 1081–1088.

[44] Kitamura, S. R., and Gómez, R. O. M. Tephra stratigraphic approach to the eruptive history of Pacaya volcano, Guatemala. *Science Reports-Tohoku University, Seventh Series. Geography 45*, 1 (1995), 1–41.

[45] Lagmay, A. M. F., and Valdivia, W. Regional stress influence on the opening direction of crater amphitheaters in Southeast Asian volcanoes. *Journal of Volcanology and Geothermal Research 158* (2006), 139–150.

[46] Lanza, F., Kenyon, L. M., and Waite, G. P. Near-surface velocity structure of Pacaya volcano, Guatemala, derived from small-aperture array analysis of seismic tremor. *Bulletin of the Seismological Society of America 106*, 4 (2016), 8.

[47] Larose, E., Derode, A., Campillo, M., and Fink, M. Imaging from the one-bit correlations of wideband diffuse wavefields. *J. Appl. Phys. 95* (2004), 8393–8399.

[48] Larose, E., Derode, A., Corennec, D., Margerin, L., and Campillo, M. Passive retrieval of Rayleigh waves in disordered elastic media. *Phys. Rev. E. 72* (2005).

[49] Levshin, A., Ratnikova, L., and Berger, J. Peculiarities of surface-wave propagation across Central Eurasia. *Bulletin of the Seismological Society of America 82*, 6 (1992), 2464–2493.

[50] Levshin, A. L., Pisarenko, V. F., and Pogrebinsky, G. A. On a frequency-time analysis of oscillations. *Ann. Geophys. 28* (1972), 211–218.

[51] Levshin, A. L., and Ritzwoller, M. H. Automated detection, extraction, and measurement of regional surface waves. *Pure Appl. Geophys. 158*, 8 (2001), 1531–1545.

[52] Levshin, A. L., Yanovskaya, T. B., Lander, A. V., Bukchin, B. G., Barmin, M. P., Ratnikova, L. I., and Its, E. N. *Seismic surface waves in a laterally inhomogeneous Earth.* V. I. Keilis-Borok, Kluwer, Norwell, Mass, 1989.

[53] Lin, F. C., Moschetti, M. P., and Ritzwoller, M. H. Surface wave tomography of the western United States from ambient seismic noise: Rayleigh and Love wave phase velocity maps. *Geophys. J. Int. 173* (2008), 281–298.

[54] Lyon-Caen, H., Barrier, E., Lasserre, C., Franco, A., Arzu, I., Chiquin, L., Chiquin, M., Duquesnoy, T., Flores, O., Galicia, O., Luna, J., Molina, E., Porras, O., Requena, J., Robles, V., Romero, J., and Wolf, R. Kinematics of the North America-Caribbean-Cocos plates in Central America from new GPS meauserements across the Polochic-Montagua fault system. *Geophysical Research Letters 33* (2006), 1–5.

[55] Mann, P., Rogers, R. D., and Gahagan, L. Overview of plate tectonic history and its unresolved tectonic problems. In *Central America: Geology, Resources, and Hazards*, J. Bundschuh and G. Alvardo, Eds., vol. 1. London, 2007, pp. 201–237.

[56] Masterlark, T., Haney, M., Dickinson, H., Fournier, T., and Searcy, C. Rheologic and structural controls on the deformation of Omkok volcano, Alaska: FEMs, InSAR, and ambient noise tomography. *Journal of geophysical Research 115* (2010), 22.

[57] Menke, W. *Geophysical Data Analysis: Discrete Inverse Theory*. Academic Press, 1984.

[58] Menke, W., and g. Jin. Waveform fitting of cross spectra to determine phase velocity using Aki's formula. *Bulletin of the Seismological Society of America 105*, 3 (2015), 1619–1627.

[59] Métaxian, J. P., Lesage, P., and Dorel, J. Permanent tremor at Masaya Volcano, Nicaragua: wavefield analysis and source location. *Journal of Geophysical Research 102* (1997), 22529–22545.

[60] Mooser, F. H., Meyer-Abich, X. X., and McBirney, A. R. *Catalogue of Active Volcanoes of the World, XI. Central America*. International Association of Volcanology, Rome, 1958.

[61] Mora, M. M., Lesage, P., Vallette, B., Alvarado, G. E., Leandro, C., Métaxian, J. P., and Dorel, J. Shallow velocity structure and seismic site effects at Anenal volcano, Costa Rica. *Journal of Volcanology and Geothermal Research 152* (2006), 121–139.

[62] Morgan, H. A., Harris, A. J. L., and Gurioli, L. Lava discharge rate estimates from thermal infrared satellite data for Pacaya Volcano during 2004-2010. *Journal of Volcanology and Geothermal Research 264* (2013), 1–11.

[63] Moriya, I. Bandaian eruption and landforms associated with it. In *Collection of articles in memory of retirement of Prof. K. Hishimura*. Tohoku University, Tokyo, 1980, pp. 214–219.

[64] Paul, A., Campillo, M., Margerin, L., Larose, E., and Derode, A. Empirical synthesis of time-asymmetrical Green function from the correlation of coda waves. *J. Geophys. Res. 110* (2005).

[65] Ren, Y., Grecu, B., Stuart, G., Houseman, G., Hegedüs, E., and Group, S. C. P. W. Crustal structure of the Carpathian-Pannonian region from ambient noise tomography. *Geophys. J. Int. 195* (2013), 1351–1369.

[66] Ritzwoller, M. H., and Levshin, A. L. Surface wave tomography of Eurasia: group velocities. *Journal of Geophysical Research 103* (1998), 4839–4878.

[67] Rodriguez, L. A., Watson, I. M., Rose, W. I., Branan, Y. K., Bluth, G. J. S., Chigna, G., Gómez, R. O. M., Escobar-Wolf, R., Carn, S. A., and Fischer, T. P. SO2 emissions to the atmosphere from active volcanoes in Guatemala and El Salvador, 1999-2002. *Journal of Volcanology and Geothermal Research 138* (2004), 325–344.

[68] Rose, W. I. Notes on fumaroles and recent activity of Volcán de Pacaya. *Geol. Bull. Ins. Geogr. Nacl. Guatemala 4* (1967), 31–33.

[69] Rose, W. I., Palma, J. L., Escobar-Wolf, R., and Gómez, R. O. M. A 50 yr eruption of a basaltic composite cone: Pacaya, Guatemala. *The Geological Society of America* (2013), 23. Special Paper 498.

[70] Russell, D. W., Herrmann, R. B., and Hwang, W. A. Application of frequency-variable filters to surface wave amplitude analysis. *Bull. Seism. Soc. Am. 78* (1988), 339–354.

[71] Sabra, K. G., Gerstoft, P., Roux, P., Kuperman, W. A., and Fehler, M. C. Extracting time-domain Green's function estimates from ambient seismic noise. *Geophysical Research Letter 32* (2005a).

[72] Sabra, K. G., Gerstoft, P., Roux, P., Kuperman, W. A., and Fehler, M. C. Surface waves tomography from microseism in southern California. *Geophysical Research Letter 32* (2005b).

[73] Saccorotti, G., Chouet, B., and Dawson, P. Shallow-velocity models at the Kilauea Volcano, Hawaii, determined from array analyses of tremor wavefields. *Geophys. J. Int. 152* (2003), 633–648.

[74] Schaefer, L. N., Oommen, T., Corazzato, C., Tibaldi, A., Escobar-Wolf, R., and Rose, W. I. An integrated filed-numerical approach to assess slope stability hazards at volcanoes: the example of Pacaya, Guatemala. *Bulletin of Volcanology 75*, 720 (2013), 18.

[75] Schaefer, L. N., Zhong, L., and Oommen, T. Post-eruption deformation processes measured using ALOS-1 and UAVSAR InSAR at Pacaya Volcano, Guatemala. *Remote Sens. 8*, 73 (2016), 15.

[76] Shapiro, N. M., and Campillo, M. Emergence of broadband Rayleigh waves from correlations of the ambient seismic noise. *Geophysical Research Letter 31* (2004).

[77] Shapiro, N. M., Campillo, M., Stehly, L., and Ritzwoller, M. H. High resolution surface wave tomography from ambient seismic noise. *Science 307* (2005), 1615–1618.

[78] Siebert, L. Large volcanic debris avalanches: characteristics of source areas, deposits, and associated eruptions. *Journal of Volcanology and Geothermal Research 22*, 3-4 (1984), 163–197.

[79] Siebert, L., Alvardo, G. E., Vallance, J. W., and van Wyk de Vries, B. Large-volume volcanic edifice failures in Central America and associated hazards. In *Volcanic hazards in Central America*, W. I. Rose, G. J. S. Bluth,

M. J. carr, J. W. Ewert, L. C. Patino, and J. W. Vallance, Eds., vol. 412. 2006, pp. 1–26. Special Papers.

[80] Snieder, R. Extracting the Green's function from the correlation of coda waves: a derivation based on stationary phase. *Phys. Rev. E. 69* (2004).

[81] Snieder, R., and Larose, E. Extracting Earth-s elastic wave response from noise measurement. *Ann. Rev. Earth Planet. Sc. 41* (2013), 183–206.

[82] Tibaldi, A. Multiple sector collapses at Stromboli Volcano, Italy: how they work. *Bulletin of Volcanology 63* (2001), 112–125.

[83] Tibaldi, A., Rust, D., Corazzato, C., and Merri, A. Setting the scene for self-destruction: From sheet intrusions to the structural evolution of rifted stratovolcanoes. *Geosphere 6*, 3 (2010), 189–210.

[84] Vallance, J. W., Siebert, L., Rose, W. I., Giron, J. R., and Banks, N. G. Edifice collapse and related hazards in Guatemala. *Journal of Volcanology and Geothermal Research 66* (1995), 337–355.

[85] Wapenaar, K. Retrieving the elastodynamic Green's function of an arbitrary inhomogeneous medium by cross-correlation. *Phys. Rev. Lett. 93* (2004).

[86] Weaver, R. L. Information from Seismic Noise. *Science 307* (2005), 1568–1569.

[87] Weaver, R. L., and Lobkis, O. I. Ultrasonic without a source: Thermal fluctuation correlation at MHz frequencies. *Phys. Rev. Lett. 87* (2001a).

[88] Weaver, R. L., and Lobkis, O. I. On the emergence of the Green's function in the correlations of a diffuse field. *J. acoust. Soc. Am. 110* (2001b), 3011–3017.

[89] Williams, H. Volcanic history of the Guatemalan Highlands. *Unvi. Calif. Berkeley, Publ. Geol. Sci. 38* (1960), 1–86.

[90] Wunderman, R. L., and Rose, W. I. Amatitlán, an actively resurging cauldron 10 km south of Guatemala City. *Journal of Geophysical Research 89* (1984), 8525–8539.

[91] Yang, Y., Ritzwoller, M. H., Levshin, A. L., and Shapiro, N. M. Ambient noise Rayleigh wave tomography across Europe. *Geophys. J. Int. 168* (2007), 259–274.

[92] Yao, H., van der Hilst, R. D., and de Hoop, M. V. Surface-wave tomography in SE Tibet from ambient seismic noise and two-station analysis: I.-Phase velocity maps. *Geophys. J. Int. 166* (2006), 732–744.

Appendix A

Aki's formula

The basic assumption of Aki [1] is that the wavefield is stochastic and stationary in time and space and it consists only surface waves, so it is designed for shallow sources and tremor [20]. Based on these hypotheses, the entire process, described in detail by the same Aki [1] and synthesized here below, involves the relation between the spectrum of the waves in time and their spectrum in space. In the exposition we focus only on the vertical component of the two-dimensional wavefield and we have decided to adopt the notation used by Ferrazzini et al. [35] and Chouet et al. [20].

Firstly, we define a spatial correlation function for a distance r between two receivers:

$$\phi(r,\varphi) = \left\langle u(x,y,t) \cdot u(x + rcos\varphi, y + rsin\varphi, t) \right\rangle \tag{A.1}$$

where the angle brackets ($\langle\rangle$) denote averaging over time, (x, y) and $(x+rcos\varphi, y+rsin\varphi)$ are the Cartesian coordinates of the two receivers and φ is the azimuth of the two receivers measured from the direction of the x axis. The azimuthal average of this function is the integral of the spatial correlation function from 0 and π:

$$\overline{\phi}(r) = \frac{1}{\pi} \int_0^{\pi} \phi(r,\varphi) d\varphi \tag{A.2}$$

For single-mode scalar waves with phase velocity $c(\omega)$, the azimuthally averaged

autocorrelation function $\overline{\phi}(r)$ of the wavefield is related to the temporal power spectrum $\Phi(\omega)$ by:

$$\overline{\phi}(r) = \frac{1}{\pi}\int_0^\infty \Phi(\omega) J_0\left[\frac{\omega}{c(\omega)}r\right] d\omega \tag{A.3}$$

where J_0 is the Bessel function of first kind and zeroth order. Note that the argument of the Bessel function may be also written as:

$$\frac{\omega}{c(\omega)}r = k(\omega)r = \frac{2\pi r}{\lambda(\omega)} \tag{A.4}$$

where $k(\omega)$ is the wavenumber and $\lambda(\omega)$ is the wavelength, both function of the angular frequency, ω. Applying a band-pass filter centered at the frequency ω_0, the power spectrum (or spectral density) of the filtered wave, $\Phi(\omega)$, becomes:

$$\Phi(\omega) = P(\omega_0)\delta(\omega - \omega_0) \qquad\qquad \omega > 0 \tag{A.5}$$

where $P(\omega_0)$ is the spectral power density at the frequency ω_0 and $\delta(\omega)$ is the Dirac delta function. Putting this expression into equation A.3, the spatial autocorrelation function becomes:

$$\overline{\phi}(r, \omega_0) = \frac{1}{\pi} P(\omega_0) J_0\left[\frac{\omega_0}{c(\omega_0)}r\right] \tag{A.6}$$

Finally, defining the autocorrelation coefficient $\rho(r, \varphi, \omega_0)$ as:

$$\rho(r, \varphi, \omega_0) = \frac{\phi(r, \varphi, \omega_0)}{\phi(0, \varphi, \omega_0)} \tag{A.7}$$

the azimuthal average of the spatial correlation function assumes the famous relation of Aki:

$$\boxed{\overline{\rho}(r,\omega_0) = J_0\left[\frac{\omega_0}{c(\omega_0)}r\right]} \tag{A.8}$$

This final expression shows that it is possible to estimate the phase velocity $c(\omega)$ of the wave as a function of frequency if one knows the correlation coefficient for a fixed r at various ω_0, because they are related through a Bessel function of the first kind and zeroth order.

Appendix B

Overlapping days

Table B.1
Overlapping days between all pairs of stations used for the cross-correlation. Stations PS02 and PS13 are not considered due to technical problems during the analyzed period.

Pair of stations	**Overlapping days (Jan 2015)**	**№ of days**
Station: **PS01**		
PS01-PS03	14-17	4
PS01-PS04	14-19	6
PS01-PS05	14-18	5
PS01-PS06	14-19	6
PS01-PS07	14-19	6
PS01-PS08	16-20	5
PS01-PS09	14-20	7
PS01-PS10	14-19	6
PS01-PS11	16-20	5
PS01-PS12	15-20	6
PS01-PS14	17-20	4
PS01-PS15	15-20	6
PS01-PS16	16-20	5

Table B.1 – continued

Pair of stations	**Overlapping days (Jan 2015)**	**Nº of days**
PS01-PS17	16-20	5
PS01-PS18	15-19	5
PS01-PS19	15-19	5
Station: **PS03**		
PS03-PS04	14-17	4
PS03-PS05	14-17	4
PS03-PS06	14-17	4
PS03-PS07	14-17	4
PS03-PS08	16-17	2
PS03-PS09	14-17	4
PS03-PS10	14-17	4
PS03-PS11	16-17	2
PS03-PS12	15-17	3
PS03-PS15	15-17	3
PS03-PS16	16-17	2
PS03-PS17	16-17	2
PS03-PS18	15-17	3
PS03-PS19	15-17	3
Station: **PS04**		
PS04-PS05	14-18	5
PS04-PS06	14-19	6
PS04-PS07	14-19	6
PS04-PS08	16-19	4
PS04-PS09	14-19	6
PS04-PS10	14-19	6
PS04-PS11	16-19	4

Table B.1 – continued

Pair of stations	**Overlapping days (Jan 2015)**	**Nº of days**
PS04-PS12	15-19	5
PS04-PS14	17-19	3
PS04-PS15	15-19	5
PS04-PS16	16-19	4
PS04-PS17	16-19	4
PS04-PS18	15-19	5
PS04-PS19	15-19	5
Station: **PS05**		
PS05-PS06	14-18	5
PS05-PS07	14-18	5
PS05-PS08	16-18	3
PS05-PS09	14-18	5
PS05-PS10	14-18	5
PS05-PS11	16-18	3
PS05-PS12	15-18	4
PS05-PS14	17-18	2
PS05-PS15	15-18	4
PS05-PS16	16-18	3
PS05-PS17	16-18	3
PS05-PS18	15-18	4
PS05-PS19	15-18	4
Station: **PS06**		
PS06-PS07	14-19	6
PS06-PS08	16-19	4
PS06-PS09	14-19	6
PS06-PS10	14-19	6

Table B.1 – continued

Pair of stations	**Overlapping days (Jan 2015)**	**Nº of days**
PS06-PS11	16-19	4
PS06-PS12	15-19	5
PS06-PS14	17-19	3
PS06-PS15	15-19	5
PS06-PS16	16-19	4
PS06-PS17	16-19	4
PS06-PS18	15-19	5
PS06-PS19	15-19	5
Station: **PS07**		
PS07-PS08	16-19	4
PS07-PS09	14-19	6
PS07-PS10	14-19	6
PS07-PS11	16-19	4
PS07-PS12	15-19	5
PS07-PS14	17-19	3
PS07-PS15	15-19	5
PS07-PS16	16-19	4
PS07-PS17	16-19	4
PS07-PS18	15-19	5
PS07-PS19	15-19	5
Station: **PS08**		
PS08-PS09	16-20	5
PS08-PS10	16-19	4
PS08-PS11	16-20	5
PS08-PS12	16-20	5
PS08-PS14	17-19	3

Table B.1 – continued

Pair of stations	**Overlapping days (Jan 2015)**	**Nº of days**
PS08-PS15	16-21	6
PS08-PS16	16-20	5
PS08-PS17	16-21	6
PS08-PS18	16-19	4
PS08-PS19	16-19	4
Station: **PS09**		
PS09-PS10	14-19	6
PS09-PS11	16-20	5
PS09-PS12	15-20	6
PS09-PS14	17-20	4
PS09-PS15	15-20	6
PS09-PS16	16-20	5
PS09-PS17	16-20	5
PS09-PS18	15-19	5
PS09-PS19	15-19	5
Station: **PS10**		
PS10-PS11	16-19	4
PS10-PS12	15-19	5
PS10-PS14	17-19	3
PS10-PS15	15-19	5
PS10-PS16	16-19	4
PS10-PS17	16-19	4
PS10-PS18	15-19	5
PS10-PS19	15-19	5
Station: **PS11**		
PS11-PS12	16-20	5

Table B.1 – continued

Pair of stations	**Overlapping days (Jan 2015)**	**Nº of days**
PS11-PS14	17-20	4
PS11-PS15	16-20	5
PS11-PS16	16-20	5
PS11-PS17	16-20	5
PS11-PS18	16-19	4
PS11-PS19	16-19	4
Station: **PS12**		
PS12-PS14	17-20	4
PS12-PS15	15-20	6
PS12-PS16	16-20	5
PS12-PS17	16-20	5
PS12-PS18	15-19	5
PS12-PS19	15-19	5
Station: **PS14**		
PS14-PS15	17-20	4
PS14-PS16	17-20	4
PS14-PS17	17-20	4
PS14-PS18	17-19	3
PS14-PS19	17-19	3
Station: **PS15**		
PS15-PS16	16-20	5
PS15-PS17	16-21	6
PS15-PS18	15-19	5
PS15-PS19	15-19	5
Station: **PS16**		

Table B.1 – continued

Pair of stations	**Overlapping days (Jan 2015)**	**Nº of days**
PS16-PS17	16-20	5
PS16-PS18	16-19	4
PS16-PS19	16-19	4
Station: **PS17**		
PS17-PS18	16-19	4
PS17-PS19	16-19	4
Station: **PS18**		
PS18-PS19	15-19	5

Appendix C

Time windows for SPAC

Table C.1
139 time windows used in the SPAC approach.

Day (Jan 2015)	StartTime (min)	EndTime (min)	Length (min)
14	105.5	110.5	5
14	512	517	5
14	773.1	778.1	5
14	888.5	893.5	5
14	124	128	4
14	545	549	4
14	603.5	608.4	4.9
14	730	734	4
14	1002	1005	3
14	1373.3	1377	3.7
14	246.3	248	1.7
14	295.8	297	1.2
14	459.2	461.5	2.3
14	515.3	518.2	2.9
14	832	835	3

Table C.1 – continued

Day (Jan 2015)	StartTime (min)	EndTime (min)	Length (min)
14	929.7	934	4.3
15	114.5	119.5	5
15	123	128	5
15	137	142	5
15	220.5	225.5	5
15	463	468	5
15	956.5	961.5	5
15	1028.5	1033.5	5
15	1424	1429	5
15	327.1	331.1	4
15	346	349.7	3.7
15	411.5	414.5	3
15	424.6	429	4.4
15	487.7	490.7	3
15	562.8	564.8	2
15	1062.8	1065.8	3
15	1183.3	1185.5	2.2
15	1415	1419	4
15	680	681	1
15	777.5	777.9	0.4
15	812.5	814.7	2.2
15	862	863.2	1.2
16	83	88	5
16	150.5	155.5	5
16	162.4	167.4	5
16	472	477	5

Table C.1 – continued

Day (Jan 2015)	StartTime (min)	EndTime (min)	Length (min)
16	735	740	5
16	828.5	833.5	5
16	967.5	972.5	5
16	995.9	1000.9	5
16	1082.5	1087.5	5
16	1090	1095	5
16	1180	1185	5
16	1252	1257	5
16	134.5	137	2.5
16	376	380	4
16	418	420	2
16	560	562	2
16	603.5	605.3	1.8
16	621.7	624	2.3
16	715	718	3
16	750	751.7	1.7
16	869.5	871.5	2
16	886	887.5	1.5
16	923	924	1
17	163.5	168.5	5
17	221	226	5
17	463	468	5
17	955.9	960.9	5
17	987	992	5
17	1080	1085	5
17	796.5	799.5	3

Table C.1 – continued

Day (Jan 2015)	StartTime (min)	EndTime (min)	Length (min)
17	875	880	5
17	992.8	994	1.2
17	995	997	2
17	923	924	1
17	1234.5	1236	1.5
18	239	244	5
18	313	318	5
18	890.7	895.7	5
18	903.7	908.7	5
18	985.5	990.5	5
18	1213.5	1218.5	5
18	1279.7	1284.7	5
18	363.5	366.5	3
18	553.5	556.7	3.2
18	1067	1071	4
18	1159.5	1163.5	4
18	1205.5	1210	4.5
18	116.5	120.5	4
18	219.5	222.5	3
18	266.7	268.5	1.8
18	301.5	306	4.5
18	465	470	5
18	636	638	2
18	664.5	667	2.5
18	789	792.5	3.5
18	818.5	821	2.5

Table C.1 – continued

Day (Jan 2015)	StartTime (min)	EndTime (min)	Length (min)
18	1050.7	1053	2.3
18	1117	1119.5	2.5
18	1142.5	1146	3.5
19	118	123	5
19	281.5	286.5	5
19	1226	1231	5
19	1333.5	1338	4.5
19	93.5	98.5	5
19	268.5	273.5	5
19	457.5	459.5	2
19	460.5	462.5	2
19	586	589	3
19	692	697	5
19	724.2	729.2	5
19	840	842	2
19	853	856	3
19	975	978	3
19	1161.1	1163	1.9
19	1324	1326	2
19	1410.5	1414.5	4
19	842.7	845	2.3
20	129	131.8	2.8
20	143	147	4
20	185	187	2
20	220	225	5
20	396.5	399	2.5

Table C.1 – continued

Day (Jan 2015)	StartTime (min)	EndTime (min)	Length (min)
20	453.1	454.1	1
20	475	480	5
20	502.5	507.5	5
20	562	565	3
20	609.5	613	3.5
20	624	629	5
20	733	734.7	1.7
20	810.2	814	3.8
20	833	834.5	1.5
20	1027.5	1030	2.5
20	1100.5	1104.5	4
20	1152	1157	5
20	1172	1178	6
20	1265.5	1268	2.5
20	1328	1333	5
21	156	158	2
21	514	517	3
21	661	667	6
21	669	672	3
21	995.5	997.5	2

Appendix D

Missed zero crossings

Table D.1
66 Missed zero crossings for the vertical-vertical (ZZ), vertical-radial (ZR) and radial-vertical (RZ) cross-correlations used for the Haney et al. [41] method. Black boxes indicate the 26 ZZ cross-correlations used for the Menke and Jin [58] technique.

Pair of stations	**ZZ**	**ZR**	**RZ**
PS01-PS03	3,4	/	1,2
PS01-PS07	/	/	4,5
PS01-PS08	/	1,2	/
PS01-PS09	/	/	1,2
PS01-PS12	/	1,2	/
PS01-PS14	/	/	/
PS01-PS15	/	3,4	1,2,4,5
PS01-PS16	2,3	2,3	/
PS01-PS17	/	/	2,3
PS01-PS18	2,3,4	/	2,3
PS01-PS19	/	4,5	2,3
PS03-PS06	/	/	3,4,5,6
PS03-PS15	1,5,6	3,4,5,6	/

Table D.1 – continued

Pair of stations	ZZ	ZR	RZ
PS03-PS16	/	/	/
PS03-PS18	/	/	/
PS03-PS19	2,3	/	/
PS04-PS06	1,2,3,4	/	/
PS04-PS07	1,2,4,5	2,3,4,5	3,4,6,7
PS04-PS08	1	4,5,7,8	/
PS04-PS10	/	/	/
PS04-PS11	3,4	/	/
PS04-PS12	6,7	3,4	/
PS04-PS19	2	3,4,5,6	3,4
PS05-PS06	1,2,3,4	/	3,4
PS05-PS09	/	2,3,5,6	3,4,6,7
PS05-PS10	/	4,5	1
PS05-PS11	/	/	/
PS05-PS12	4,5	/	/
PS05-PS16	1,3,4,5,6	1,2,5,6	/
PS05-PS17	1,2,5,6,7,8	1,2	/
PS06-PS10	/	3,4	1
PS06-PS11	1	/	/
PS06-PS15	/	/	3,4
PS06-PS17	1,2,5,6	1,2,3,4	2,3
PS07-PS10	3,4	2,3	5,6
PS07-PS11	1	/	/
PS07-PS12	/	/	6,7
PS07-PS14	2,3,5,6	/	/
PS07-PS15	/	1,2	1

Table D.1 – continued

Pair of stations	ZZ	ZR	RZ
PS08-PS09	/	/	1,2
PS08-PS10	/	/	1,2
PS08-PS11	3,4	4,5	2,3
PS08-PS12	/	4,5	1,3,4
PS08-PS14	/	1	/
PS08-PS15	/	/	/
PS08-PS16	1,2	/	1
PS08-PS19	2,3	/	/
PS09-PS10	/	/	/
PS09-PS12	/	2,3	/
PS09-PS15	2,3,4,5	5,6	/
PS09-PS16	3,4	/	1,4,5
PS09-PS17	/	/	/
PS09-PS19	/	/	/
PS10-PS14	/	/	/
PS10-PS15	3,4	/	2,3
PS10-PS16	/	2	/
PS10-PS17	/	/	3,4
PS10-PS18	2,3	3,4	/
PS10-PS19	/	3,4	/
PS11-PS14	/	/	/
PS11-PS15	/	3,4	5,6
PS11-PS16	3,4	/	/
PS11-PS18	/	1,2	/
PS11-PS19	/	1,2,5,6	/
PS12-PS14	/	4,5	/

Table D.1 – continued

Pair of stations	ZZ	ZR	RZ
PS12-PS17	2,3	/	2,3
PS12-PS18	/	/	2,3
PS12-PS19	/	/	2,3
PS14-PS15	2,3,4,5	/	4,5
PS14-PS17	/	2,3	/
PS14-PS18	3,4	/	/
PS14-PS19	/	3,4	4,5
PS15-PS16	1,3,4,5,6	/	4,5
PS15-PS17	/	/	1,3,4
PS16-PS17	1,2	/	3,4
PS16-PS18	1,2,3,4	3,4	/
PS16-PS19	1,2,4,5	1,2,4,5	2,3,4,5
PS17-PS19	2,3	2,3	/

Appendix E

Ekström-Menke: phase velocity - distance relationship

Table E.1
Phase velocities (in km/s) as a function of frequency (expressed in Hz) found through the comparison of 26 dispersion curves between the Ekström et al. [34] method and the Menke and Jin [58] grid search. The subscript of the phase velocity indicates the estimation of the velocity at that frequency: *0.5*, *1.0*, *1.5*, *2.0*, *2.5* and *3.0* Hz.

Pair of stations	**D (km)**	$v_{0.5}$	$v_{1.0}$	$v_{1.5}$	$v_{2.0}$	$v_{2.5}$	$v_{3.0}$
PS01-PS07	1.3144	2.6	2.0	1.6429	1.5286	1.413	1.3
PS01-PS08	0.65375	1.6	1.15	0.7	0.8	0.9	1.0
PS01-PS09	0.56025	2.5	1.9	1.3	1.0	1.0	1.0
PS01-PS12	0.36795	2.7	2.06	1.42	1.04	0.92	0.8
PS01-PS14	0.36328	2.8	2.0	1.2	0.78	0.74	0.7
PS01-PS15	1.1697	2.4	1.92	1.44	1.22	1.26	1.3
PS03-PS16	1.0094	3.0	2.0667	1.5571	1.4714	1.3857	1.3
PS03-PS18	0.57258	1.7	1.3	0.9	0.8	0.9	1.0
PS05-PS09	1.2904	3.0	1.5	1.425	1.35	1.275	1.2
PS06-PS15	1.0979	3.0	2.44	1.88	1.62	1.66	1.7
PS07-PS12	1.4357	3.0	1.7	1.6	1.5	1.4	1.3

Table E.1 – continued

Pair of stations	D (km)	$v_{0.5}$	$v_{1.0}$	$v_{1.5}$	$v_{2.0}$	$v_{2.5}$	$v_{3.0}$
PS07-PS15	0.42885	2.8	2.04	1.28	0.88	0.84	0.8
PS08-PS14	0.36959	1.0	0.8	0.6	0.56	0.68	0.8
PS09-PS10	0.31399	1.3	1.02	0.74	0.64	0.72	0.8
PS09-PS12	0.64853	2.2	1.64	1.08	0.86	0.98	1.1
PS10-PS14	0.42056	2.0	1.48	0.96	0.66	0.58	0.5
PS10-PS16	1.1769	1.9	1.62	1.34	1.18	1.14	1.1
PS10-PS17	0.96508	1.9	1.58	1.26	1.12	1.16	1.2
PS10-PS19	1.4169	3.0	1.2	1.2	1.2	1.2	1.2
PS11-PS14	0.76157	2.2	1.96	1.72	1.48	1.24	1.0
PS11-PS19	0.93707	1.8	1.44	1.08	0.92	0.96	1.0
PS12-PS14	0.56949	2.1	1.74	1.38	1.14	1.02	0.9
PS12-PS18	0.88895	1.7	1.4	1.1	1.0667	1.0333	1.0
PS12-PS19	1.1656	2.4	1.3	1.275	1.25	1.225	1.2
PS14-PS17	0.57562	1.5	1.18	0.86	0.68	0.64	0.6
PS15-PS17	1.0604	2.9	1.9	1.413	1.4429	1.4714	1.5

Appendix F

Haney et al. method: phase velocity - distance relationship

Table F.1
Phase velocities (in km/s) as a function of frequency (expressed in Hz) found with the Haney et al. [41] method of 66 dispersion curves. The subscript of the phase velocity indicates the estimation of the velocity at that frequency: *0.5*, *1.0*, *1.5*, *2.0*, *2.5* and *3.0* Hz.

Pair of stations	**D (km)**	$v_{0.5}$	$v_{1.0}$	$v_{1.5}$	$v_{2.0}$	$v_{2.5}$	$v_{3.0}$
PS01-PS03	0.62663	1.667	0.9860	0.7252	0.5832	0.4925	0.4290
PS01-PS08	0.65375	0.9097	0.7908	0.7286	0.6875	0.6572	0.6334
PS01-PS15	1.1697	2.1722	1.6416	1.3936	1.2407	1.1337	1.0532
PS01-PS16	0.62731	0.8707	0.7057	0.6241	0.5720	0.5346	0.5059
PS01-PS17	0.51874	0.8213	0.6657	0.5887	0.5396	0.5043	0.4772
PS01-PS18	0.9983	1.7686	1.2462	1.0155	0.8781	0.7846	0.7155
PS01-PS19	1.3456	1.9073	1.4414	1.2236	1.0894	0.9954	0.9247
PS03-PS06	1.6714	2.6027	2.0370	1.7650	1.5943	1.4734	1.3814
PS03-PS15	1.6564	2.0323	1.7668	1.6278	1.5359	1.4682	1.4151
PS03-PS19	0.79824	1.0559	0.8559	0.7569	0.6937	0.6484	0.6135
PS04-PS06	1.2437	1.2239	1.1411	1.0953	1.0640	1.0403	1.0213

Table F.1 – continued

Pair of stations	D (km)	$v_{0.5}$	$v_{1.0}$	$v_{1.5}$	$v_{2.0}$	$v_{2.5}$	$v_{3.0}$
PS04-PS07	1.8006	1.8833	1.5265	1.3500	1.2373	1.1564	1.0943
PS04-PS08	2.0358	1.9114	1.6617	1.5310	1.4445	1.3809	1.3309
PS04-PS10	1.4689	1.6549	1.3413	1.1863	1.0872	1.0161	0.9615
PS04-PS11	1.4849	1.8610	1.4064	1.1939	1.0629	0.9712	0.9023
PS04-PS12	1.6722	2.0332	1.5365	1.3044	1.1612	1.0611	0.9857
PS04-PS19	1.5149	2.4812	1.9419	1.826	1.5199	1.4046	1.3169
PS05-PS06	0.54414	0.6736	0.5856	0.5395	0.5091	0.4866	0.4690
PS05-PS09	1.2904	1.6734	1.3564	1.1995	1.0994	1.0275	0.9723
PS05-PS10	1.2343	1.8752	1.3213	1.0766	0.9311	0.8318	0.7586
PS05-PS11	1.5107	1.9249	1.3564	1.1052	0.9557	0.8539	0.7788
PS05-PS12	1.5959	2.0188	1.3263	1.0374	0.8714	0.7612	0.6815
PS05-PS16	2.2664	2.1633	2.0170	1.9361	1.8806	1.8387	1.8052
PS05-PS17	2.0248	1.6900	1.5215	1.4309	1.3698	1.3243	1.2882
PS06-PS10	1.1239	1.6461	1.2012	0.9990	0.8766	0.7920	0.7290
PS06-PS11	1.5584	1.7043	1.3814	1.2217	1.1197	1.0465	0.9902
PS06-PS17	1.7890	1.7445	1.5165	1.3972	1.3184	1.2602	1.2147
PS07-PS09	0.79249	1.2998	0.9159	0.7463	0.6454	0.5766	0.5259
PS07-PS10	1.0336	1.2782	1.0360	0.9162	0.8398	0.7849	0.7427
PS07-PS11	1.5479	1.7470	1.4665	1.3237	1.2310	1.1635	1.1112
PS07-PS12	1.4357	1.7231	1.4464	1.3057	1.2142	1.1477	1.0960
PS07-PS14	0.95764	1.1806	0.9910	0.8945	0.8319	0.7863	0.7509
PS08-PS09	0.46543	0.6727	0.6056	0.5695	0.5452	0.5271	0.5127
PS08-PS10	0.75349	1.6625	1.1311	0.9030	0.7696	0.6799	0.6144
PS08-PS11	1.1274	1.7550	1.3263	1.1259	1.0024	0.9159	0.8509
PS08-PS12	0.9291	1.5627	1.1011	0.8972	0.7759	0.6932	0.6322
PS08-PS14	0.36959	0.6439	0.5405	0.4879	0.4537	0.4289	0.4096

Table F.1 – continued

Pair of stations	D (km)	$v_{0.5}$	$v_{1.0}$	$v_{1.5}$	$v_{2.0}$	$v_{2.5}$	$v_{3.0}$
PS08-PS15	0.55128	1.0199	0.7708	0.6543	0.5825	0.5323	0.4945
PS08-PS16	1.0110	2.8128	1.9820	1.6150	1.3966	1.2477	1.1380
PS08-PS19	1.9124	3.3381	2.6126	2.2637	2.0448	1.8897	1.7717
PS09-PS15	0.75123	1.0424	0.8158	0.7069	0.6385	0.5901	0.5532
PS09-PS17	0.80572	2.0253	1.6416	1.4518	1.3306	1.2436	1.1768
PS10-PS14	0.42056	1.9123	1.1311	0.8320	0.6691	0.5620	0.4921
PS10-PS15	1.0541	1.3276	1.0761	0.9517	0.8722	0.8152	0.7714
PS10-PS16	1.1769	1.5621	1.4565	1.3980	1.3580	1.3277	1.3035
PS10-PS17	0.96508	1.8905	1.2863	1.0269	0.8752	0.7731	0.6987
PS10-PS18	1.1270	1.6919	1.3714	1.2128	1.1116	1.0389	0.9830
PS10-PS19	1.4169	1.9760	1.5465	1.3400	1.2104	1.1186	1.0488
PS11-PS15	1.5444	1.9736	1.4915	1.2661	1.1272	1.0300	0.9569
PS11-PS16	1.0425	1.6487	1.3363	1.1818	1.0832	1.0123	0.9579
PS11-PS18	0.72993	1.4173	1.0711	0.9092	0.8094	0.7397	0.6871
PS11-PS19	0.93707	1.3585	1.1011	0.9738	0.8925	0.8341	0.7893
PS12-PS17	0.87912	1.3429	1.0511	0.9107	0.8226	0.7602	0.7128
PS12-PS18	0.88895	1.4250	1.1962	1.0798	1.0041	0.9491	0.9064
PS12-PS19	1.1656	1.5323	1.2863	1.1611	1.0797	1.0206	0.9747
PS14-PS15	0.82274	0.9880	0.8008	0.7082	0.6491	0.6066	0.5740
PS14-PS16	0.90881	1.6050	1.4965	1.4364	1.3953	1.3642	1.3393
PS14-PS17	0.57562	0.8293	0.8008	0.7846	0.7733	0.7646	0.7576
PS14-PS18	1.2947	2.1129	1.8368	1.6924	1.5968	1.5264	1.4712
PS14-PS19	1.5892	2.0749	1.7417	1.5722	1.4621	1.3820	1.3198
PS15-PS16	1.5574	1.8722	1.5716	1.4186	1.3192	1.2469	1.1908
PS15-PS17	1.0604	1.7413	1.4114	1.2482	1.1440	1.0692	1.0117
PS16-PS17	0.51572	1.5301	1.0410	0.8311	0.7083	0.6257	0.5655

Table F.1 – continued

Pair of stations	D (km)	$v_{0.5}$	$v_{1.0}$	$v_{1.5}$	$v_{2.0}$	$v_{2.5}$	$v_{3.0}$
PS16-PS18	1.0611	1.1285	1.0160	0.9555	0.9147	0.8843	0.8602
PS16-PS19	1.4981	1.5660	1.3614	1.2543	1.1835	1.1313	1.0904
PS17-PS19	1.7608	2.9037	2.4374	2.2002	2.0460	1.9339	1.8469